[Papers in Palaeontology, 2018, pp. 1–32]

# POSTCRANIAL MORPHOLOGY OF THE EARLY TRIASSIC EPICYNODONT *GALESAURUS PLANICEPS* (OWEN) FROM THE KAROO BASIN, SOUTH AFRICA

*by* ELIZE BUTLER[1,2], FERNANDO ABDALA[3,4] *and* JENNIFER BOTHA-BRINK[1,2]

[1]Karoo Palaeontology, National Museum, PO Box 266, Bloemfontein, 9300, South Africa; elize.butler@nasmus.co.za; jbotha@nasmus.co.za
[2]Department of Zoology & Entomology, University of the Free State, Bloemfontein, 9300, South Africa
[3]Evolutionary Studies Institute & School of Geosciences, University of the Witwatersrand, Private Bag 3, WITS 2050, Johannesburg, South Africa; nestor.abdala@gwits.ac.za
[4]Unidad Ejecutora Lillo, CONICET, Miguel Lillo 251, Tucumán, Argentina

Typescript received 13 October 2017; revised 14 March 2018; accepted in revised form 5 April 2018

**Abstract:** The Early Triassic non-mammaliaform epicynodont *Galesaurus planiceps* formed an important part of ecosystems following the Permo-Triassic Mass Extinction, the greatest mass extinction in Phanerozoic history. Here, we re-examine the postcranial skeleton of *Galesaurus* and present data which sheds light on the biology, ecology and possible survival strategies of this species. We find evidence for two distinct morphotypes, a gracile and a robust morph, which we interpret as stages in an ontogenetic series. The primary differences between the morphs manifest in the girdles, with further subtle differences in the fore and hind limbs. Our study also reveals postcranial differences between *Galesaurus* and the contemporaneous taxon *Thrinaxodon liorhinus*, allowing these taxa to be distinguished in the absence of cranial material. We also report the first evidence of intraspecific variation in the presence and distribution of disc-like phalanges in a non-mammaliaform cynodont. An analysis of the osteohistology of *Galesaurus* reveals rapid growth to skeletal maturity within one year, thereafter transitioning to slow intermittent growth. This growth pattern is similar to that of *Thrinaxodon*, which also grew rapidly and continuously to skeletal, and possibly reproductive, maturity within its first year of life. Features such as a strong, reinforced pelvis, elongated ilium, thick, robust forelimbs and stout unguals indicate that *Galesaurus* was capable of actively excavating burrows. The combination of rapid maturation and fossoriality may have aided its survival in the harsh, unpredictable post-extinction Early Triassic environment.

**Key words:** Epicynodontia, morphology, osteohistology, Permo-Triassic Mass Extinction, *Galesaurus planiceps*.

THE South African Karoo Basin is well-known for its extraordinary preservation of Permo-Triassic therapsids (Rubidge & Sidor 2001; Rubidge 2005), the extinct relatives of mammals that include non-mammaliaform cynodonts. The latter group comprises fossil forms closely related to living mammals (Rowe 1988; Wible 1991; Hopson & Kitching 2001), and provides one of the main sources of data on the origin and evolution of mammals (Abdala 2007; Botha *et al.* 2007; Liu & Olsen 2010; Ruta *et al.* 2013). Early representatives of non-mammaliaform cynodonts (hereinafter referred to as cynodonts) were key players in the ecosystems before and after the most catastrophic mass extinction in Phanerozoic history: the Permo-Triassic Mass Extinction (PTME) (Abdala & Ribeiro 2010; Botha-Brink *et al.* 2012; Smith & Botha-Brink 2014). The basal epicynodont *Galesaurus planiceps* (Owen, 1859) formed an important part of the Early Triassic post-extinction ecosystem in the Karoo Basin. Its lowest occurrence is in the upper part of the Lower Triassic Palingkloof Member, Balfour Formation and it has a short biostratigraphical range into the lowermost part of the overlying Katberg Formation, corresponding to approximately the lower half of the *Lystrosaurus* Assemblage Zone (LAZ) (Botha-Brink *et al.* 2012).

The cranial anatomy of this species is reasonably well known (Broom 1932*a*; Parrington 1934) and partial postcranial elements have been briefly described (Haughton 1924; Parrington 1934; Kemp 1969; Jenkins 1971; Panko 2001). The taxon is characterized by the presence of an incomplete osseous secondary palate and unique postcanines with the first postcanine having only one cusp and the rest two cusps, the main (mesial) cusp being remarkably curved with a posteriorly-directed tip (Broom 1932*a*, *b*; Hopson & Kitching 1972; Jasinoski & Abdala 2017*a*). In


doi: 10.1002/spp2.1220

the last two decades, the number of *Galesaurus* specimens has increased substantially and now includes superb, completely articulated skeletons (e.g. Abdala *et al.* 2006, fig. 3; Botha & Smith 2006, fig. 4). Thus, 13 individuals of this taxon are documented by a large portion of the skeleton. The postcrania of cynodonts (as is the case in most therapsids) have received far less attention than the crania (e.g. Bonaparte 1963; Jenkins 1970). A short account of *Galesaurus* by Parrington (1934), described several postcranial remains, but only four cervical vertebrae were definitely associated with a *Galesaurus* skull. The most extensive publication on cynodont postcrania continues to be the monograph by Jenkins (1971) on the postcrania of South African cynodonts in which he provided a comparative description of four South African taxa. It includes a comprehensive description of the postcrania of *Thrinaxodon liorhinus*, a contemporaneous taxon of *Galesaurus* and one of the best represented cynodonts in the Karoo Basin (Jasinoski *et al.* 2015). Since this monograph, limited research on the postcrania of African cynodonts has been produced (Kemp 1980*a*, *b*; Gow 2001; Blob 2001, 2006; Sues & Jenkins 2006; Kammerer *et al.* 2008; Gaetano *et al.* 2017) whereas a string of recent contributions have described the postcrania of various cynodont taxa from the Brazilian Triassic (e.g. Oliveira 2010; Oliveira *et al.* 2007, 2009, 2010; Oliveira & Schultz 2016) and from a Laurasian traversodontid (Liu *et al.* 2017).

The aim of this study is to provide new information on the biology and ecology of the epicynodont *Galesaurus planiceps* by conducting a comprehensive morphological and osteohistological analysis of its postcranial skeleton. The abundance of postcranial material now available for this taxon allows us to address: (1) intraspecific variation in the morphology of the adult postcrania; (2) ontogenetic variation in the morphology and osteohistology of the postcrania; and (3) similarities/differences with the contemporaneous taxon *Thrinaxodon liorhinus*. *Thrinaxodon* specimens are conspicuously more abundant than those of *Galesaurus* and it has a notably longer biostratigraphical range, extending most of the way through the LAZ. Recent behavioural studies (Jasinoski & Abdala 2017*b*) have hinted at possible reasons for the better success of *Thrinaxodon*, but this topic has yet to be fully explored. New data from this study may shed light on possible drives for the selective advantage of one taxon, which has important implications for the biology and ecology of the Early Triassic cynodonts living in a post-extinction environment.

## MATERIAL AND METHOD

We examined the morphology of 16 specimens, including the articulated, nearly complete skeletons of 3 specimens (Table 1). Measurements of basal skull length (BSL) and postcranial elements are presented in Table 2. The ontogenetic age of the individuals was estimated by comparing the BSL against the largest known specimen of *Galesaurus* (NMQR 860; Table 2) and is expressed as a percentage of maximum known size (% of maximum BSL known). NMQR 860, 3542 and SAM-PK-K10468 are considered to be adults based on morphology (Butler 2009; Jasinoski & Abdala 2017*a*) and osteohistology (Butler 2009). Skulls less than 67 mm were not available for study. Several specimens of *Thrinaxodon*, comprising partial or complete skeletons, were also examined for comparison (MMK 5265; BP/1/472, 1693, 1730, 3848, 4331, 5208; the digitally prepared BP/1/7199, Fernandez *et al.* 2013; TM 80A; SAM-PK-K1395, 8004, 10017, 10607; USNM 22812). In both *Galesaurus* and *Thrinaxodon*, juveniles are allocated to 0–39% maximum known size (hereinafter referred to as % size for brevity), sub-adults 40–79% and adults 80–100% (Jasinoski & Abdala 2017*a*). It is worth noting here that the *Galesaurus* specimen NMQR 135 comprises a multi-aged aggregation of at least four individuals. There are two smaller skulls with only the occipital region preserved and two larger skulls, one of which is almost complete and the other a partial skull with the posterior region preserved. The almost complete skull is missing only the left zygomatic arch (labeled here as NMQR 135a in Table 2). It is assumed that it is the one typically used in other studies on *Galesaurus* as the other skulls are not complete enough to provide any useful measurements. Given that the BSL of NMQR 135a is 94 mm and is thus, 82% of the maximum known BSL, it is considered to be an adult. The skulls and postcrania are not articulated and thus none of the postcranial elements can be assigned to any particular skull. However, the sizes of the scapula, procoracoid and coracoid, which were used in the morphological analysis, are similar to those of other adult individuals. A humerus within the aggregation was found to be too small to belong to one of the larger adult skulls. It is 65% the length of the largest humerus in the sample (compared against the right humerus of NMQR 860, Table 2) and probably belongs to one of the smaller skulls, indicating that although these skulls are too incomplete to be measured, they are probably subadults and that this aggregation contains two age classes. Interpretation of muscle attachments on the bones are based on Jenkins (1971), Kemp (1980*a*, *b*), Oliveira & Schultz (2016) and Lai *et al.* (2018).

Four of the study specimens were included in the osteohistological analysis. The material for thin sectioning comprises a tibia and fibula from RC 845 (61% adult), a humerus from the NMQR 135 aggregation (65% adult), a femur from NMQR 3716 (63% adult), and the humerus, radius, ulna, femur and tibia from NMQR 3542 (89% adult). The bones were embedded under vacuum in a clear epoxy resin (Epofix) and left to cure for 24 hours.

**TABLE 1.** *Galesaurus planiceps* postcranial material examined in this study.

| Accession No. | Material | Farm, District |
|---|---|---|
| BP/1/4506 | Skull and articulated left humerus, radius, ulna, manus and scapula, vertebrae, ribs, parts of the pelvic girdle, femora, tibiae, fibulae, and left and right pes | Fairydale, Bethulie |
| BP/1/2513 | Block with one large and two small skulls. Large specimen A includes cervical and lumbar vertebrae, scapula, interclavicle, left clavicle, thoracic and lumbar ribs, complete left forelimb, including articulated manus, right humerus, disarticulated metacarpals and phalanges. Specimen B comprises anterior cervical vertebrae, partial right forelimb and left manus. Specimen C includes anterior cervical vertebrae, procoracoid, coracoid, clavicles, interclavicle, articulated radius and ulna, partially articulated ribs, articulated thoracic and caudal vertebrae, partial pelvic girdle, hind limb | Unknown |
| BP/1/5064 | Skull and several postcranial fragments, including vertebrae, parts of manus or pes | Fairydale, Bethulie |
| BP/1/4714 | Skull and several postcranial fragments including right scapula, coracoid fragment, interclavicle, vertebrae, ribs and partial left humerus | Draycot, Escourt |
| NMQR 135 | An almost complete large skull (specimen A), another partial large skull and another two partial smaller skulls. Fragmentary postcrania, including a disarticulated scapulocoracoid and a complete humerus | Oviston area, Venterstad |
| NMQR 3340 | Skull and partial limb bone | Rietpoort, Dewetsdorp |
| NMQR 3542 | Skull and disarticulated left scapula, vertebrae, ribs, femora, humeri, radii, left ulna, left tibia and fibula, part of pelvis and portions of the manus or pes | Fairydale, Bethulie |
| NMQR 860 | Skull and disarticulated postcranial skeleton including vertebrae, scapulae, humeri, left and right skapulocoracoid, interclavicles, left radius and partial ulna, right partial radius and ribs | Harrismith |
| NMQR 3716 | Five blocks: Block one with poorly preserved posterior skull and posterior left mandible, articulated cervical, thoracic and lumbar vertebrae, left iluim, femur, tibia, fibula and partial left pes; Block two with one skull without skull roof, axis, atlas and cervicals; Block three with articulated thoracic vertebrae and ribs, right scapula and humerus, left partial distal humerus; Block four with lumbar vertebrae, ilia, left femur; Block five with poorly preserved skull without mandible and skull roof | Fairydale, Bethulie |
| RC 845 | Skull and almost complete articulated postcranial skeleton; excluding the radii, ulnae, left femur, left tibia, left fibula, manus and pes | Fairydale, Bethulie |
| UMZC T819 | Skull and cervical vertebrae | Harrismith |
| UMZC T823 | Fragment of the skull, femur, humerus and isolated vertebra | Harrismith |
| SAM-PK-K10465 | Skull and complete articulated postcranial skeleton with dislodged caudal vertebrae | Fairydale, Bethulie |
| SAM-PK-K10468 | Skull and disarticulated postcranial skeleton, including scapulae, complete right and partial left humeri, vertebrae, clavicles, partial interclavicle, complete right radius and partial right ulna and left manus | Fairydale, Bethulie |
| SAM-PK-K1119 | Complete skull and disarticulated postcranial elements, thoracic vertebrae, left scapula, partial left humerus, radii and ulnae | Harrismith |
| TM 83 | Skull and disarticulated scapulae, vertebrae, rib fragments, femora, humeri, right radius, ulnae, tibiae and fibulae | James' Donga Harrismith |

The blocks were then serially sectioned and the slices adhered to frosted glass slides using the same resin. The sections were ground further using a Struers Accutom-100 and polished to approximately 60 μm thick. The resulting thin sections were then digitally rendered under ordinary, polarized (PL), and cross-polarized light (CPL; i.e. polarized light with lambda compensator) using a Nikon Eclipse Ci polarizing microscope and DS-Fi3 digital camera in NIS-Elements 4.5 (Nikon Corp.). Osteohistological terminology and definitions follow those of Francillon-Vieillot *et al.* (1990) and Ricqlès *et al.* (1991).

As cortical vascularization is closely related to bone apposition rate (e.g. Amprino 1947; Margerie *et al.* 2002) being able to quantitatively compare between different bone elements and taxa provides a standardized method for comparing bone depositional rates. The relative vascular area was quantified using the image analysis program NIS Elements D 4.5 (Nikon Corp.). It was calculated by taking the total canal area and dividing it by the total cortical area for each field of view around the mid-cortex and then multiplying by 100 to obtain a percentage. This method produces the maximum possible vascularization for each element, as the channels would have included lymph and nerves as well as blood vessels during life (Starck & Chinsamy 2002).

Images of transverse sections from the centre of the midshaft were converted into black and white and analysed in Bone Profiler (Girondot & Laurin 2003) to

**TABLE 2.** Cranial and postcranial measurements (in mm) of *Galesaurus planiceps*.

| | SAM-PK-10465 | RC 845 | SAM-PK-K1119 | NMQR 3716 | BP/1/4506 | BP/1/2513a | NMQR 135a | NMQR 3542 | SAM-PK-K10468 | NMQR 860 |
|---|---|---|---|---|---|---|---|---|---|---|
| % Adult | 59 | 61 | 63 | 63 | 75 | 79 | 82 | 89 | 92 | 100 |
| Basal skull length | 67 | 69 | 72 | 75 | 85 | 90 | 94 | 102 | 105 | 114 |
| **Scapulocoracoid length** (left/right) | 34.2/27.3 | – | ~38.4 R | – | 42/51.3 | – | – | 38.9 | – | 51.8/45.7 |
| **Humerus** (left/right) | | | | | | | | | | |
| Total length | 42.5/41.2 | 39.8 L | – | 41.7 R | 52.2 L | 54.4/54.1 | 39.5 L | 57.9 R | – | 51.3/60.7 |
| Proximal width | 18.3/18.8 | 16.5/17.4 | – | 12.8 R | 15.7 L | 21.0 R | 16.4 L | 13.9 R | 19.3/21.2 | 22.5/24.2 |
| Distal width | 12.0/12.9 | – | 17.8 R | – | 24.5 L | 27.6 R | 20.5 L | 25.8 R | ~16 R | 27.3/24.3 |
| **Radius** (left/right) | | | | | | | | | | |
| Total length | 34.3 R | – | 27.6/32.0 | – | 39.7 L | 40.8 L | – | 42.5 L | 35.7 R | 37.2 L |
| Proximal width | 9.8/10.1 | – | 6.1/7.9 | – | 7.6 L | 11.2 L | – | 11.7 L | 5.3 R | 10.8 L |
| Distal width | 9.0/9.1 | – | 6.3/7.3 | – | – | 10.8 L | – | 10.2 L | 7 R | 10.4 L |
| **Ulna** (left/right) | | | | | | | | | | |
| Total length | 35.7/32.2 | – | ~26.6/~26.9 | – | 40.7 L | – | – | 53.0/51.7 | – | – |
| Proximal width | 7.0/9.1 | – | 8.7/7.3 | – | 8.4 L | – | – | 13/8.4 | 7.2 R | – |
| Distal width | 6.5/4.8 | – | 4.5/4.8 | – | 10.8 L | – | – | 9.2/9.3 | – | – |
| **Pelvis** | | | | | | | | | | |
| Length of the iliac plate | 39.0 R | 38.4 | – | 39.0/38.5 | 41.4/44.3 | – | – | – | – | – |
| Length of pubic plate | – | 13.2 | – | – | 23.8 R | – | – | – | – | – |
| Length of ischial plate | – | 18.2 R | – | – | – | – | – | – | – | – |
| **Femur** (left/right) | | | | | | | | | | |
| Total length | 46 R | 44.3 L | – | 46.4/45.4 | 58.2 L | – | – | 61.5/61.5 | – | – |
| Proximal width | 13.9/12.4 | – | – | 16.6 L | 18.3/19.9 | – | – | 15 L | – | – |
| Distal width | 14/14.3 | – | – | 12.4/10 | 15/16 | – | – | 17.4/18.4 | – | – |
| **Tibia** (left/right) | | | | | | | | | | |
| Total length | 39.4 R | – | – | – | ~40.1/44.2 | – | – | 54 R | – | – |
| Proximal width | 8.5/9.5 | – | – | – | 5.2 L | – | – | 12.2 R | – | – |
| Distal width | – | – | – | – | 11.3/9.7 | – | – | – | – | – |
| **Fibula** (left/right) | | | | | | | | | | |
| Total length | 38.8/36.3 | – | – | – | 39.8/39.7 | – | – | 52.6/~51.4 | – | – |
| Proximal anteroposterior length | 6.6/7.9 | – | – | – | 16.0/17.3 | – | – | 8.8 L | – | |
| Distal anteroposterior length | 6.9/4.8 | – | – | – | 7.3/7.3 | – | – | 9.5 L | – | – |

Individuals above 80% maximum known size are considered to be adults. Specimen NMQR 135 comprises at least four disarticulated individuals; the skull (labeled 'a') and humerus listed here probably do not belong to the same individual (see text for details). *Abbreviations*: L, left side; R, right side.

quantify the cortical thickness for comparison between elements and with other taxa. The thickness of the bone wall has biomechanical implications and may thus provide information on the lifestyle adaptation of the animal (Laurin *et al.* 2011). Global compactness (Cg), which measures the ratio of bone tissue present within a bone cross-section (as opposed to the space represented by the medullary cavity, resorption cavities etc.; Girondot & Laurin 2003) and *K* value, which measures the ratio of the inner and outer diameters of the bone (where *k* tends towards 0 when the bone walls are thin and tends towards 1 when the bone walls are thick; Currey & Alexander 1985) were obtained from Bone Profiler and provide quantifiable measures of comparison.

*Institutional abbreviations.* BP, Evolutionary Studies Institute (formerly Bernard Price Institute for Palaeontological Research), University of the Witwatersrand, Johannesburg, South Africa; MMK, McGregor Museum, Kimberley, South Africa; NMQR, National Museum, Bloemfontein, South Africa; RC, Rubidge Collection, Wellwood, Graaff-Reinet, South Africa; SAM-PK-K, Iziko South African Museum, Cape Town, South Africa; TM, Ditsong: National Museum of Natural History, Pretoria, South Africa; UMZC, University Museum of Zoology, Cambridge, UK; USNM, National Museum of Natural History, Smithsonian Institution, Washington DC, USA.

## DESCRIPTION

Basal skull lengths (BSL) range from 67 to 114 mm (Table 2, see also Jasinoski & Abdala 2017*a*). Based on the general morphology of the skulls and associated postcrania, two distinct morphs were recognized: a small, gracile morph and a large robust morph. Individuals with a BSL from 50 to 79% of the largest specimen (NMQR 860) are considered to be subadults, whereas those from 80 to 100% are considered to be adults (Table 2). Individuals smaller than 50% of the maximum known size have yet to be discovered. In each case, the BSL of the gracile morphs falls within the size range of 67–90 mm (< 80% adult), whereas robust morphs all have a BSL above ~94 mm (≥ 80% adult), indicating that the two morphs form an ontogenetic series with the gracile morphs representing ontogenetically younger individuals and the robust morphs older individuals. The description of *Galesaurus planiceps* is compared with that of the closely related *Thrinaxodon liorhinus*.

### *Axial skeleton*

The axial skeleton of both *Galesaurus* and *Thrinaxodon* is differentiated into five regions (Jenkins 1971). The presacral count of *Thrinaxodon* is 27 (MMK 5265, BP/1/7199), although one specimen has 24 or 25 presacrals (TM 171). The final count for this specimen cannot be confirmed due to poor preservation. The number of presacrals in *Galesaurus* varies from 25 (RC 845) to 29 (SAM-PK-K10465, BP/1/4506). SAM-PK-K10465 preserves 7 cervical, 15 thoracic, 7 lumbar, 6 sacral and at least 25 caudal vertebrae (Fig. 1). Specimen RC 845 is represented by 7 cervical, 11 thoracic, 7 lumbar and only 5 preserved caudal vertebrae (Figs 2, 3). The presacral count in this specimen should be considered with caution as the two blocks in which the specimen is preserved do not connect perfectly, and thus it is possible that a few thoracic vertebrae were not preserved. The vertebral count of the presacral vertebrae in *Galesaurus* is thus 7 cervical, ?11–15 thoracic and 7 lumbar vertebrae, to which should be added at least 25 caudal vertebrae.

*Axis.* There is a ridge that runs along the anterior surface of the axial neural spine. The latter becomes progressively higher posteriorly (Fig. 4A, C). The posterior tip of the spine is laterally expanded in both subadult (RC 845, NMQR 3716) and adult specimens (NMQR 3542, BP/1/5064) (Fig. 4C). The most notable difference between the two morphotypes is that the neural spine of the smaller individuals is directed more posteriorly and is shorter than those of the large specimens. The posterior margin of the spine is expanded laterally in specimens of all sizes. The prezygapophysis, present in all the axis vertebrae in our sample, projects as a small blunt process (Fig. 4A, C, D). The atlas centrum of adult NMQR 3542 is anteriorly convex (Fig. 4A, E). The lateral facet for the atlas neural arch is preserved in this specimen. The dens is observed as a faint point in subadult RC 845 (Fig. 5). In this specimen, a clear line represents the fusion of the atlas and axis centra. The postzygapophyses are more developed than the prezygapophyses and have an inclination of 25–30° from the horizontal (Fig. 4A, B). The transverse processes of the axis are directed posterolaterally (as observed by Jenkins 1971 in *Galesaurus* UMC 2721) and slightly ventrally (Fig. 4D, F), having a similar length to the transverse processes of the remaining cervicals.

The atlas arch in subadult RC 845 (Fig. 5) is exposed in posteromedial view and has a low-lying lamina and a large simple facet for the atlas articulation. The posterior portion of the lamina has a small swollen area, in the same region where Jenkins (1971, fig. 3C) described a groove. The transverse process of the atlas has a broad base and is directed ventrally. There is an anterior process at the base of the lamina that we interpret as the articulation with the proatlas.

*Proatlas.* The left proatlas in subadults SAM-PK-K10468 and RC 845, the right in SAM-PK-K 10465 and both in NMQR 3716 are preserved close to their natural position. The proatlas can only be described in dorsal view due to the manner in which it is preserved in all specimens. As mentioned by Parrington (1934), it is supported posteriorly by the atlas arch. The proatlas is a sub-rectangular bone (Fig. 5) with a posterolaterally directed process. In SAM-PK-K10468, the process sits at an angle of 50–60° from the long axis of the bone.

*Cervical series.* The neural spines of the cervical vertebrae are tall (Fig. 2A). In subadult RC 845, the posterior margin of the neural spines of the fourth and fifth vertebrae is concave, whereas the

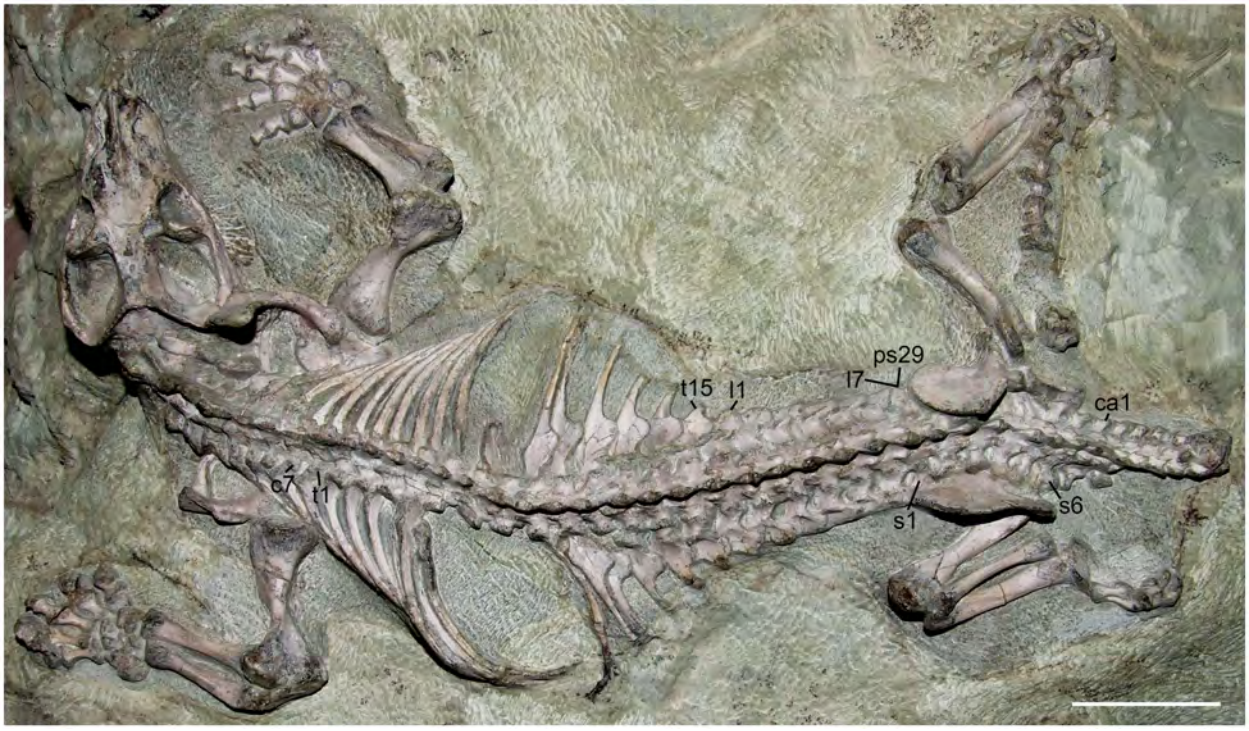


**FIG 1.** Skeleton of *Galesaurus planiceps*, SAM-PK-K-10465. Vertebral count by region is: 7 cervical (c); 15 thoracic (t); 7 lumbar (l); (29 presacral (ps)); 6 sacral (s); and at least 25 caudal (ca) vertebrae. Scale bar represents 40 mm. Colour online.

neural spines of the sixth and seventh vertebrae are directed more posteriorly and their posterior margin is less curved (Fig. 2A). The intercentra between vertebrae 6, 7 and 8 are absent, however Parrington (1934, text-fig. 3) described intercentra between the first four cervical vertebrae. The transverse processes are stout and oriented posterolaterally, whereas the process of the seventh vertebra is laterally oriented (Fig. 2A) and, because of this change, it is considered to be the last cervical vertebra. A similar lateral orientation of the transverse processes is observed in the seventh vertebra of subadult BP/1/4506. The neural spines of the adult SAM-PK-K10468 are tall and curved, whereas the transverse processes are directed more laterally than those in subadult RC 845. In the latter specimen, the laterally positioned zygapophyseal articulation sits at the same low angle as it does in the axis. This articulation becomes more medially oriented to the extent that between the eighth and ninth vertebrae (the first two thoracics) the zygapophyses surround the base of the neural spine. This change in zygapophyseal position is first observed between the seventh and eighth vertebrae in subadult BP/1/4506. Anapophyses in subadult RC 845 are present in all presacral (Fig. 2B) and caudal vertebrae, as well as one sacral vertebra. A clear suture between the centra and neural arches of the vertebrae is present in RC 845, reaffirming that it was not fully grown at the time of death. Other studies have suggested very late fusion of the neurocentral sutures in theriodonts (Sigurdsen *et al.* 2012; Huttenlocker & Botha-Brink 2014).

*Thoracic series.* The tallest neural spine in subadult RC 845 is that of the first thoracic, whereas the neural spine of the second thoracic vertebra is slightly shorter (Fig. 2A). From there on, the neural spines remain at a similar height (or slightly lower than the anterior ones) until the second sacral vertebra. The neural spines of the last cervical and first thoracic are roughly rectangular in lateral view, with the posterior margins curving posteriorly. The anterodorsal margin of the spine in the ninth thoracic vertebra, and in those posterior to this bone (including the lumbar vertebrae), are convex in lateral view (Figs 2, 3). The tips of the thoracic and lumbar neural spines are more robust and more elongated anteroposteriorly than those of the cervicals.

The transverse processes of the fourth thoracic vertebra are shorter than those of the anterior elements (Fig. 3) and are directed laterally or slightly anteriorly. The zygapophyseal articular facets are more vertical than those of the cervicals and are oriented more medially at the base of the spine. The zygapophyses become more horizontally oriented between the eighth and ninth thoracic vertebrae, becoming more vertical again in the last lumbar vertebra. In contrast to *Thrinaxodon* (Jenkins 1971, p. 54), subadult RC 845 has no posterior displacement of the transverse process in relation to the vertebral body in the posterior thoracic and lumbar vertebrae.

*Lumbar series.* Seven lumbar vertebrae are recognized in subadult RC 845 (Fig. 3). The neural spines of the lumbar vertebrae are triangular to semi-triangular in transverse section and become progressively more robust posteriorly. The transverse processes are well-developed and the lumbar plates remain fused to the processes.

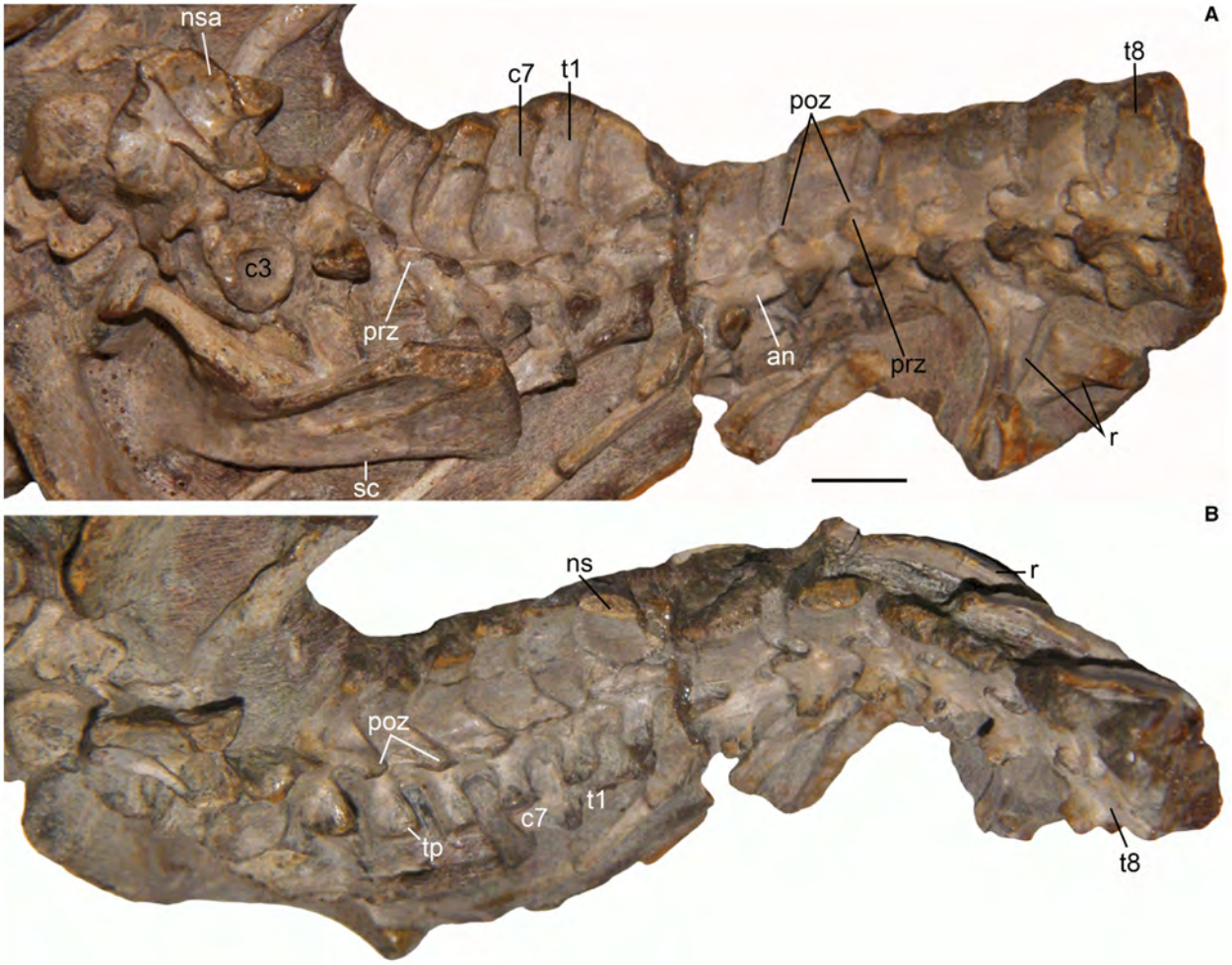


**FIG. 2.** Anterior vertebral sequence of *Galesaurus planiceps*, RC 845: A, lateral; B, dorsal views of the anterior vertebral column until vertebra 15. Vertebral count is: 7 cervical (c); 8 thoracic (t) vertebrae. *Abbreviations*: an, anapophysis; ns, neural spine; nsa, neural spine of the atlas; poz, postzygapophysis; prz, prezygapophysis; r, rib; sc, scapula; tp, transverse process. Scale bar represents 10 mm. Colour online.

*Sacral series.* Five sacral vertebrae are preserved in subadult RC 845 in which the neural spine becomes progressively shorter posteriorly. The zygapophyseal articular facets are vertically oriented at the base of the neural spine. It is possible to observe the presence of an anapophysis in the first sacral vertebra. In SAM-PK-K10465, six sacral vertebrae are present (Fig. 6A); the transverse processes of the first to the fifth vertebrae are short and shaped like an hourglass. However, the processes of the sixth sacral vertebra are shaped slightly differently where they contact the ilium through a long anterior projection and the posterior portion forms a short, rounded process (Fig. 6A).

*Caudal series.* Five caudal vertebrae are preserved in subadult RC 845 and at least 25 in SAM-PK-K10465. In the latter specimen, 6 of the proximal vertebrae are in articulation (Fig. 6A) whereas two detached articulated portions contain 8 and 11 vertebrae (Fig. 6B). Transverse processes are present in the anterior six vertebrae of SAM-PK-K10465 (Fig. 6A) and RC 845. Anapophyses are present, but they are considerably smaller than those of the presacral and sacral elements. In the series of 11 vertebrae, the first 4 are as wide as long, whereas the posterior elements are longer than wide (Fig. 6B).

*Ribs*

In subadult NMQR 3716, the atlantal and axial ribs are wide, thin plates, whereas those in the fully articulated subadult SAM-PK-K10465 have spatulate proximal ends. SAM-PK-K10465 preserves unexpanded ribs until the 14th vertebra (7th thoracic). Ribs are not preserved with the eighth vertebra (Fig. 1), whereas the next six ribs (from the 9th to the 14th thoracic vertebra) preserve plates and a distal unexpanded portion. The following eight ribs (15th to 22nd thoracic vertebrae) preserve plates without the distal unexpanded portions and are interpreted as lumbar ribs. RC 845 has unexpanded ribs until vertebra 15 (8th thoracic), whereas the next four (9th to 12th thoracic vertebrae)

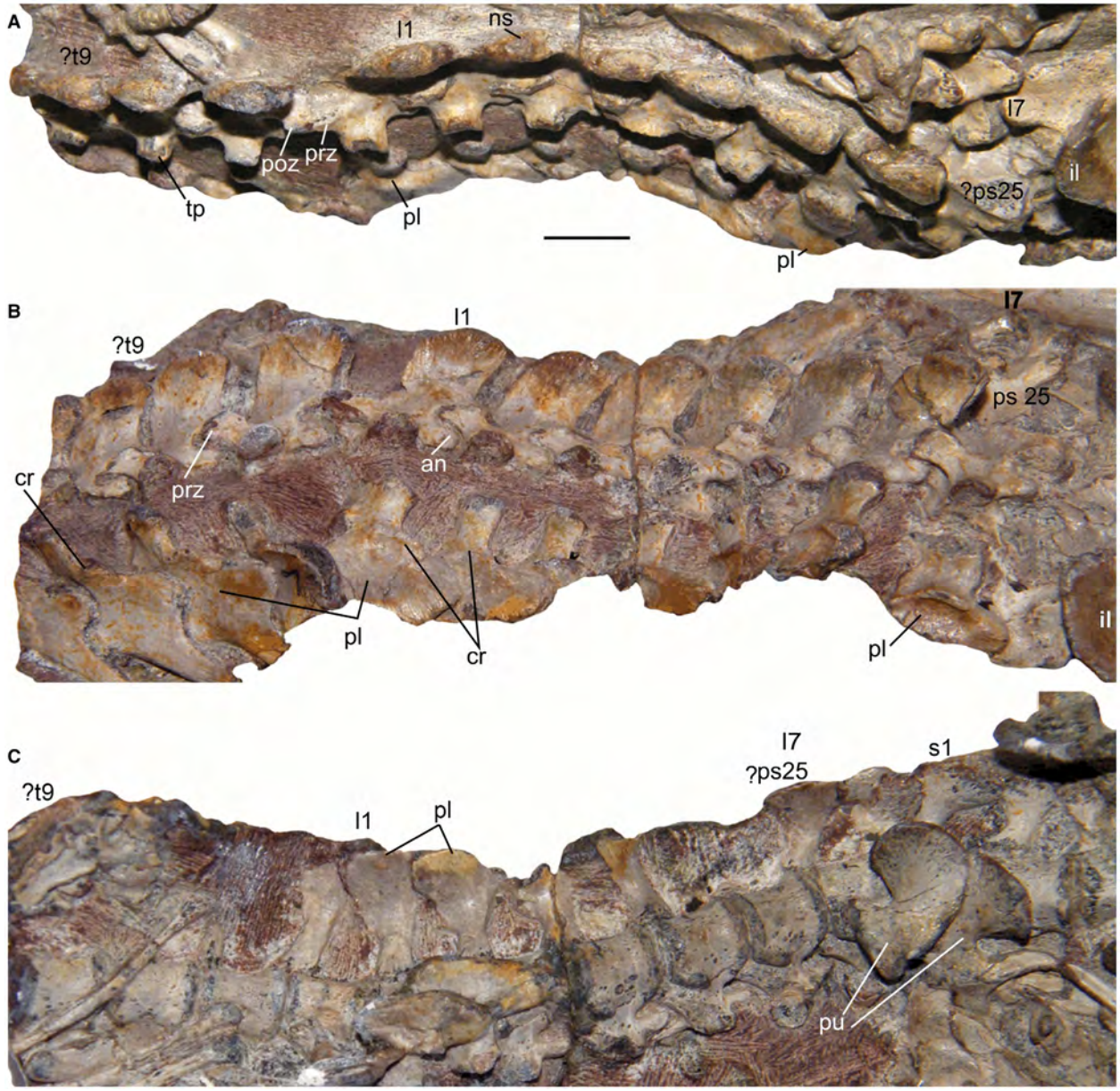


**FIG. 3.** Posterior vertebral sequence of *Galesaurus planiceps*, RC 845: A, dorsal; B, lateral; C, ventral view of the posterior vertebral column from vertebra thoracic ?9 (?t9) until the first sacral vertebra (s1). Vertebral count is: 3 thoracic (t); 7 lumbar (l) and 1 sacral vertebrae; (?25 presacral vertebrae (?ps25)). *Abbreviations*: an, anapophysis; cr, costal ridge; il, ilium; ns, neural spine; pl, costal plate; poz, postzygapophysis; prz, prezygapophysis; ps, presacral vertebrae; pu, pubis; tp, transverse process. Scale bar represents 10 mm. Colour online.

have plates with the distal unexpanded portions, and the following seven lumbar ribs have only plates.

*Cervical ribs.* In lateral view, the cervical ribs terminate proximally in a thin triangular plate formed by the separation of the capitulum and tuberculum, which are not distinct processes, but continuous with the rib shaft. The cervical ribs are directed posterolaterally and ventrally, tapering distally. The capitulum and tuberculum lie in close proximity, with the former being ventral and slightly anterior to the latter. The tuberculum is oriented medioventrally and slightly anteriorly. The dorsal margin of the cervical ribs is continuous with the tuberculum and shows a dorsal convexity in the area where, in posterior elements, the costal plates would have developed. Parrington (1934) described the atlantal rib of *Galesaurus* as long and distally expanded.

*Dorsal ribs.* In subadult RC 845, the capitulum and tuberculum of the anterior dorsal ribs are more separated than those in the

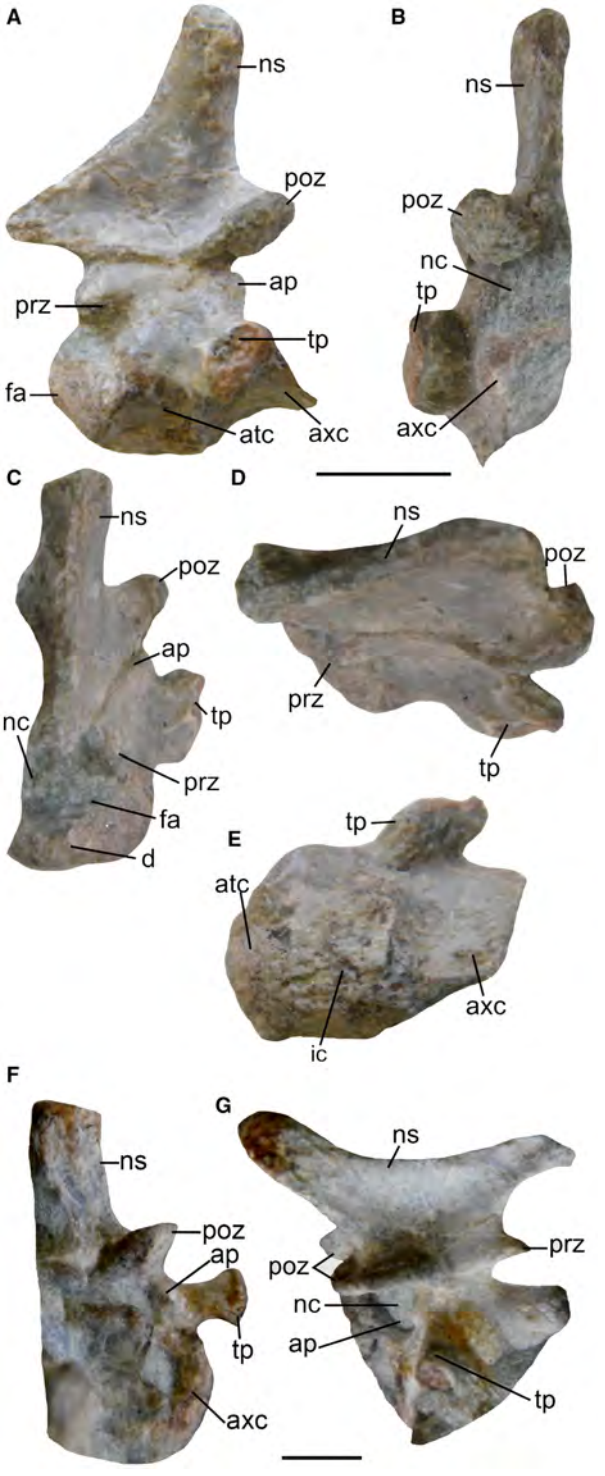


**FIG. 4.** Atlas and axis of *Galesaurus planiceps*. A–E, NMQR 3542: A, lateral; B, posterior; C, anterior; D, dorsal; E, ventral view. F–G, BP/1/5065: F, posterior; G, lateral view. *Abbreviations*: ap, anapophysis; atc, atlas centrum; axc, axis centrum; d, dens; fa, facet for atlas arch; ic, intercentrum; nc, neural canal; ns, neural spine; poz, postzygapophysis; prz, prezygapophysis; tp, transverse process. Scale bars represent: 10 mm (A–E); 5 mm (F, G). Colour online.

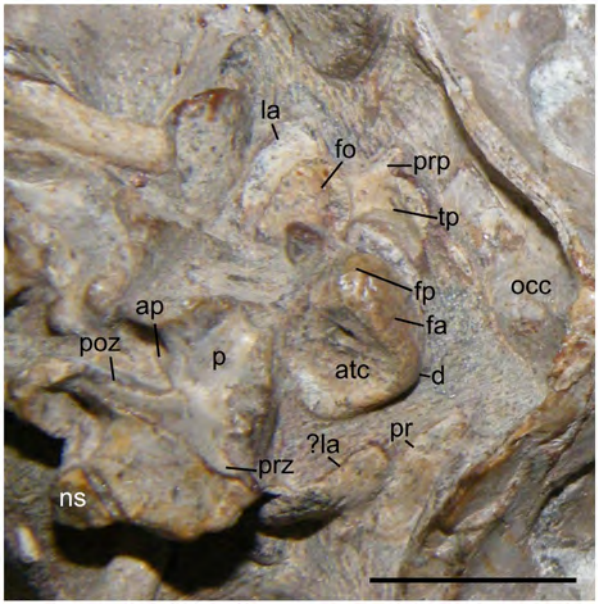


**FIG. 5.** Atlas and axis of *Galesaurus planiceps* RC 845 in dorsal view. *Abbreviations*: ap, anapophysis; atc, atlas centrum; d, dens; fa, facet for atlas arch; fo, facet for occipital condyle; fp, facet for axis pedicle; la, atlas arch lamina; ns, neural spine; occ, occiput of the skull; p, pedicle; poz, postzygapophysis; pr, proatlas; prp, process for articulation with proatlas; prz, prezygapophysis; tp, transverse process. Scale bar represents 5 mm. Colour online.

central dorsal ribs. In the triangular proximal area of the central dorsal ribs (posterior ribs without plates) a ridge is visible on the anterior surface. This ridge is well developed in the adult NMQR 860, the largest specimen in our sample.

The posterior dorsal ribs have a proximal rectangular plate, which then narrows posteriorly and ventrally as an unexpanded rib (Figs 1, 3). There is a rounded and incipient costal tubercle immediately distal to the dorsal articulation of the rib associated with the transverse process. The distal portion of the rib shortens progressively and disappears in vertebra 17 (10th thoracic) (Fig. 1).

*Lumbar ribs.* Jenkins (1971) described all lumbar ribs as having no distal rib shaft. According to this definition, seven lumbar vertebrae and ribs are recognized in subadult RC 845. These ribs are costal plates that are dorsoventrally oriented and are oval to irregular in shape. The costal tubercle forms a low anteroposteriorly directed ridge, immediately distal to the articulation of the rib with the vertebra. The heads converge and the proximal portion of the rib that articulates with the vertebra is relatively robust.

*Caudal ribs.* The most anterior caudal rib in subadult RC 845 has a broad base and a bifurcated distal portion with a posterior projection larger than the anterior one. The following ribs appear as thin plates without bifurcation. In the adult SAM-PK-K10465, the most anterior caudal rib is also bifurcated and the posterior projection is relatively larger than the anterior one (Fig. 1). In the second caudal rib, the anterior projection is

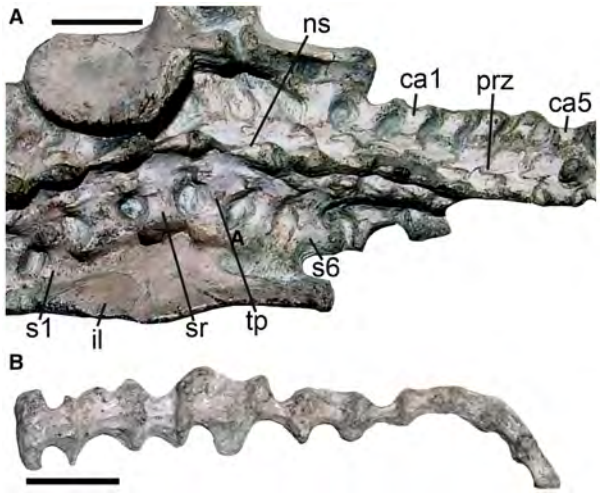


**FIG. 6.** Sacral and caudal vertebrae of *Galesaurus planiceps* SAM-PK-K10465. A, sacral and first five caudal vertebrae. B, last caudal vertebra. *Abbreviations*: ca, caudal vertebra; il, ilium; ns, neural spine; prz, prezygapophysis; s, sacral vertebra; sr, sacral rib; tp, transverse process. Scale bar represents 10 mm. Colour online.

reduced to a process, and in the following elements the rib is a single structure (probably only represented by the posterior projection).

*Anterior appendicular skeleton*

*Scapulocoracoid.* The scapula of subadult RC 845 (Fig. 7A, B) comprises a long, narrow lamina that is bowed laterally (particularly on the anterior margin) and posteriorly expanded in the posterodorsal border. The scapular blade in the largest specimen, NMQR 860, is also remarkably expanded in its posterodorsal margin (Fig. 7C, D). The margins of the blade show various degrees of lateral bowing in the larger specimens, being less marked in NMQR 860 compared to NMQR 3542. This difference may be due to deformation in the former specimen. The dorsal border of the scapular blade is nearly straight and has numerous striations (particularly prominent in NMQR 3542) indicating strong muscular attachment. The striations in *Thrinaxodon* (NMQR 809) are less pronounced. The posterior and particularly the anterior margins of the blade are raised to form the infraspinous fossa (Oliveira & Schultz, 2016; Lai *et al.* 2018), which is deepest across the anterior section of the scapular blade. In subadult specimens SAM-PK-K10465 and RC 845, a prominent bony ridge extends dorsoventrally on the center of the lateral surface of the scapular blade (Fig. 7A, B). This bony ridge may represent the origin of the M. infraspinatus. There is no evidence of the groove for the origin of M. teres major on the thickened dorsoposterior edge of the scapula (Jenkins 1971, fig. 17D). In anterior view, the anterior margin forms a noticeable convexity, which is directed laterally where the acromial area is located (Fig. 6B). Butler (2009) described the acromion process in specimen NMQR 135 as a thickening on the averted edge of the scapula that terminates in a small protrusion anteriorly. Jenkins (1971) noted that the acromion process was not developed in *Thrinaxodon*, because in all well-preserved specimens the averted edge is very thin and appears complete. However, he did describe a local thickening of the bone edge that could represent the point of acromioclavocular articulation.

The base of the scapula of one of the larger individuals from the NMQR 135 aggregation consists of a supraglenoid buttress that bears a semi-circular articulation facet forming the dorsal portion of the glenoid, and a procoracoid buttress, both of which are located on the medial side of the scapular base and are separated by a shallow canal. The procoracoid buttress is longer than the supraglenoid buttress and has a straight suture with the scapula. In subadult RC 845, the scapular surface of the glenoid is slightly convex and faces posterolaterally and ventrally. The triangular coracoid in NMQR 135 is joined to the procoracoid by a jagged suture, directed dorsoventrally (Fig. 7E). The posterior margin of the coracoid in NMQR 135 shows a high tip representing the tuberosity for attachment of the triceps.

The ventral border of the procoracoid-coracoid complex has a rugose texture for the attachment of the M. biceps (Jenkins 1971). Two fossae are present on the medial side of the procoracoid–coracoid complex: a depression on the coracoid, which is deepest at the coracoid–procoracoid suture, and extends onto the lateral surface of the procoracoid, and a second, shallower oval fossa, on the medial surface of the procoracoid that lies adjacent to the anteroventral margin of the bone.

The procoracoid is slightly larger than the coracoid (Fig. 7E). A rounded, large foramen, oriented slightly posterodorsally, is present in the largest specimen NMQR860. The procoracoid–coracoid of NMQR 135, only visible in medial view, shows that the procoracoid foramen opens medially into the shallow canal that separates the supraglenoid from the procoracoid buttresses. The thickest part of shoulder girdle is where the scapula, coracoid and procoracoid contact each other to form the glenoid.

*Clavicle.* As is commonly found in cynodonts (Jenkins 1970, 1971; Oliveira *et al.* 2010) the proximal portion of the clavicle in the adult NMQR 860 is a spoon shaped plate (Fig. 8B). Parallel striations are visible on the exposed ventral surface of the left clavicle. In subadult RC 845, more prominent striations are present on the dorsal surface of this plate (Fig. 8C). The anterior margin of the plate varies from straight to slightly convex, whereas the posterior margin is strongly convex. The proximal portion of the left clavicle of NMQR 860 is plate-like and becomes progressively thicker distally until it becomes a shaft-like bone that curves dorsally at an angle of 40° from the horizontal (Fig. 8A). The most distal portion expands again, but to a lesser degree than the proximal plate, and forms a concave area in contact with the acromial region of the scapular blade.

*Interclavicle.* The complete interclavicle is preserved in subadult RC 845, whereas only the anterior portion is preserved in the largest, adult specimen NMQR 860. The interclavicle is a cruciate bone with a long posterior ramus (Fig. 8D, E). Four ridges extend from an anterior central tuberosity; two laterally, one anteriorly and a longer posterior ridge. The lateral and anterior ridges create a bilateral, triangular depression for the reception of the medial ends of the clavicles. The posterior ridge is clearly

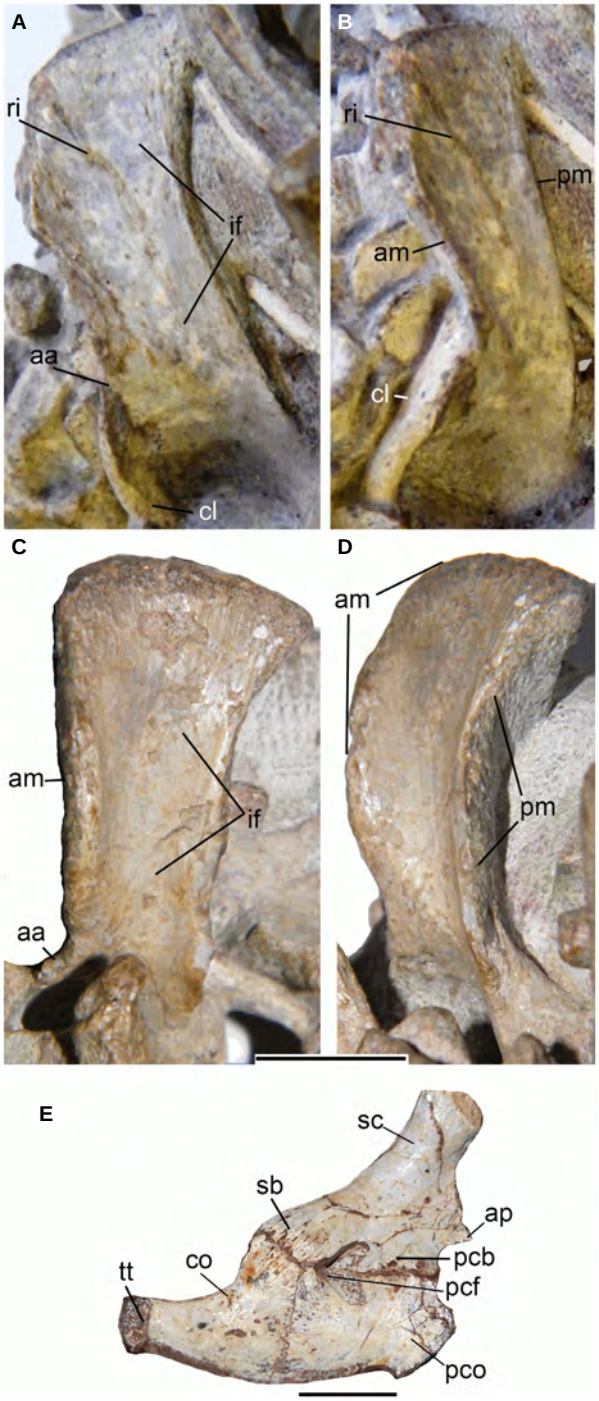


**FIG. 7.** Shoulder girdle of *Galesaurus planiceps*. A–B, left scapula of RC 845: A, lateral; B, anterolateral view. C–D, left scapula of NMQR 3542: C, lateral; D, posterolateral view. E, left procoracoid, coracoid and base of the scapula of NMQR 135 in medial view. *Abbreviations*: aa, acromial area; ap, acromial process; am, anterior margin; cl, clavicle; co, coracoid; if, infraspinous fossa; pco, procoracoid; pcb; procoracoid buttress; pcf, procoracoid foramen; pm, posterior margin; ri, ridge; sb, supraglenoid buttress; sc, scapula; tt, tuberosity for origin of the M. triceps. Scale bars represents 10 mm. Colour online.

defined anteriorly, but gradually fades posteriorly. The long posterior ramus has fine striations indicating muscle attachment and gradually narrows to form a thin oval-shaped distal end. The interclavicle of NMQR 860 (apart from being more robust than RC 845) shows a progressive convergence of the lateral margins of the posterior ramus, immediately posterior to the lateral ridges (Fig. 8E), whereas, in RC 845, these margins are subparallel (Fig. 8D).

*Humerus.* Complete and partial humeri of 13 specimens are represented in our sample. This element shows two expanded ends connected by a narrow central shaft (Abdala 1999). The distal end of the humerus is wider than the proximal although there is a large variation (from 53% to 81%). Wider distal ends of the humeri are represented in all non-mammaliaform cynodonts (Abdala 1999, table 4).

The dorsally-oriented humeral head is smooth and only slightly convex in proximal view (Fig. 9A). The articulation facet on the head in *Galesaurus* is strap-shaped and the lesser tuberosity is slightly thicker than the greater tuberosity (Fig. 9A, B). The anterior surface expands onto the deltopectoral crest, which is angled at approximately 120° to the longitudinal axis in proximal view. The crest is ~51% of the length of the bone in the adult NMQR 3542 a similar ratio to that of *Procynosuchus*, *Thrinaxodon* and some gomphodont cyndonts (Abdala 1999, table 4). This ratio is comparatively shorter in the small specimen RC 845 (~40%). Striations, probably for the insertion for the M. infraspinatus, are present on the proximal surface of the deltopectoral crest (Fig. 9D), whereas the insertion for the M. dorsoscapularis (i.e. M. deltoideus) is situated slightly distally in anterolateral view. A shallow, but broad fossa is present on the anterolateral surface of the deltopectoral crest and probably indicates the origin of the M. brachialis (Fig. 9C). A possible insertion for the M. teres minor is represented by a ridge that separates the broad fossa from the humeral head. A second low and uneven ridge extends across the dorsal surface of the humeral shaft and may have been the area of insertion for the M. latissimus dorsi (Fig. 9D). A well-developed bicipital groove extends from the proximal ventral surface, narrowing until it disappears approximately halfway down the length of the humerus (Fig. 9A).

The triangular central shaft, connecting the proximal and distal ends, is short and slender in most specimens, apart from the adult NMQR 860, which is relatively robust (Fig. 9C).

In ventral aspect, the triangular distal end of the humerus is asymmetrical because the bulbous entepicondyle is displaced farther from the radio-ulnar facet than the ectepicondyle (Fig. 9B, E). In smaller specimens the entepicondyle is thicker than the ectepicondyle, similar to that seen in *Thrinaxodon* (Jenkins 1971). In contrast, this condition is reversed in large specimens of *Galesaurus* (e.g. NMQR 3542 where the ectepicondyle is 35% thicker than the entepicondyle). This differs from that observed in the smaller specimens and instead agrees with Jenkins' (1971) description of *Galesaurus* in which the entepicondyle is thicker. The ovoid entepicondylar foramen is twice the size of the circular ectepicondylar foramen and is enclosed by a flange with a slightly swollen border. The trochlea in the centre of the distal end extends onto the dorsal margin of the bone.

*Radius.* This bone is cylindrical and expands towards the epiphyses with the proximal end being notably more expanded than the distal end (Fig. 10A). In lateral view, the anterior margin of the bone is slightly convex, whereas the posterior margin is concave. This concavity is produced by the expansion of the proximal articular facet and the tuberosity that contacts the ulna distally. The proximal end has an anteroposteriorly concave articulation surface that slopes medially as is seen in *Thrinaxodon* (Jenkins 1971). The proximal end of the radius from subadult SAM-PK-K1119 (Fig. 10B) has a shallow depression the outline and orientation of which resembles that of larger cynodonts (Jenkins 1971). In the adult NMQR 3542, a tuberosity with an articulation facet for the radial notch of the ulna is present on the posterolateral surface of the proximal end. A posterior ridge, visible only on the midshaft (due to poor preservation), passes from the ulnar facet distally along the side of the shaft. Jenkins (1971) noted a prominent swelling at the midpoint of the posterior ridge and interpreted it as the radial tuberosity for the insertion of the M. biceps as observed in large cynodonts. This feature is also present in NMQR 3542. A vertically-oriented fossa, medial to the radial tuberosity, may represent the insertion of the M. flexor digitorum superficialis (Jenkins 1971). The radius of NMQR 3542 preserves the region for the distal tuberosity for the ulnar contact, but it was not observed in this bone. The distal end of the radius forms a flat surface and is expanded both lateromedially and anteroposteriorly.

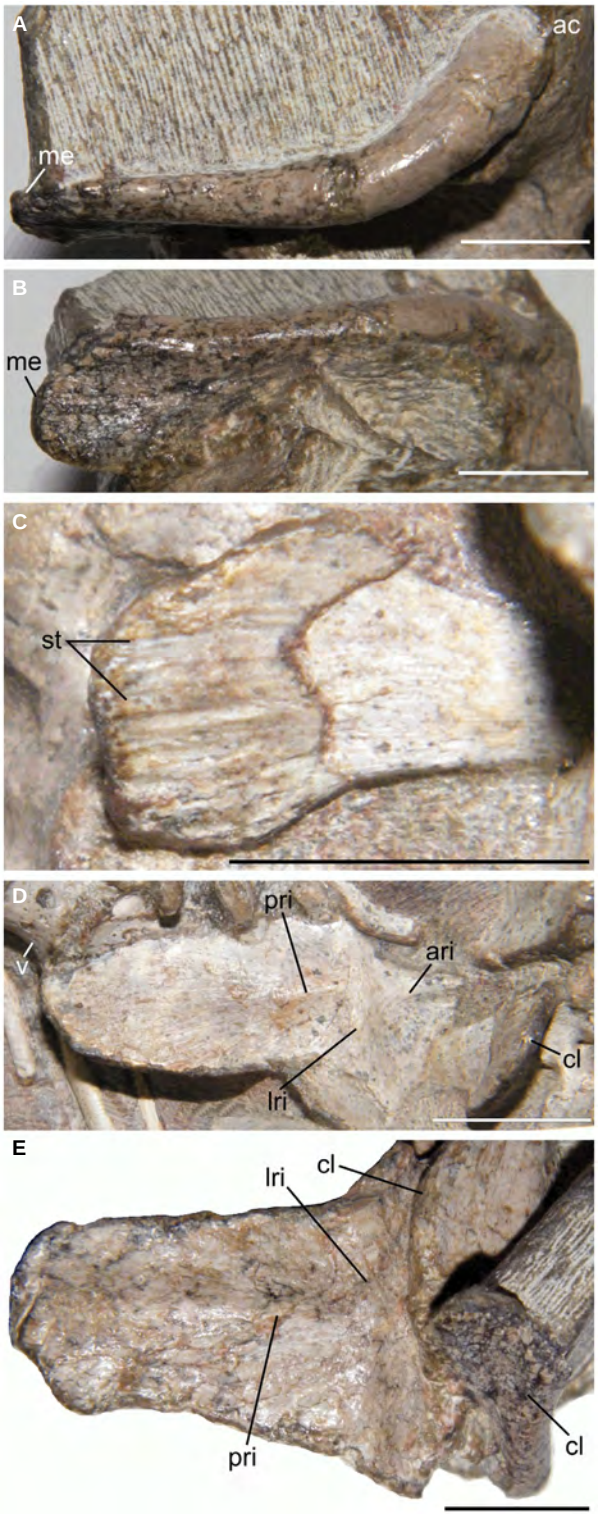


*Ulna.* The ulna is a slender bone, with a lateromedially-flattened shaft and a poorly developed distal end compared to that of the radius (Fig. 10A). The presence of a high, anteromedial ulnar crest that extends distally along 90% the length of the shaft, results in the bone appearing broad in lateral view. Subadult SAM-PK-K1119 has a distinctive ulnar crest that ends close to the distal end of the bone (Fig. 10C). The crest widens just below the proximal articular surface of the ulna and narrows again, approximately two-thirds of the way down the bone shaft.

The proximal end expands laterally, being wider than the distal end. The facet for the humerus is oval and slants anteriorly and slightly laterally towards the shaft axis. Ossification of the bone on the anteromedial margin appears to be incomplete or cancellous in the subadults. An olecranon process is absent. Two articulation facets for the radius are observed on the proximal end in lateral view: a spoon-shaped anterior fossa, which attenuates sharply distally and terminates between the middle and distal third of the ulna, and a smaller radial notch on the posterior surface. The posterior fossa is better developed than the radial notch. The distal end is slightly longer laterally than medially, and slopes medially.

*Manus.* Most of the description is based on subadult SAM-PK-K10465 and NMQR 3716 (Fig. 10A, B). There are ten bones in the carpus (Fig. 11B, C) arranged in three rows: the proximal

**FIG. 8.** Clavicle and interclavicle of *Galesaurus planiceps*. A, anterior view of left clavicle NMQR 860. B, ventral view of left clavicle NMQR 860. C, ventral view of the proximal portion of left clavicle RC 845. D, ventral view of interclavicle RC 845. E, ventral view of interclavicle NMQR 860. *Abbreviations*: ac, acromial portion; ari, anterior ridge; cl, clavicle; lri, lateral ridge; me, medial margin; pri, posterior ridge; st, striations; v, vertebra. Scale bar represents 10 mm. Colour online.

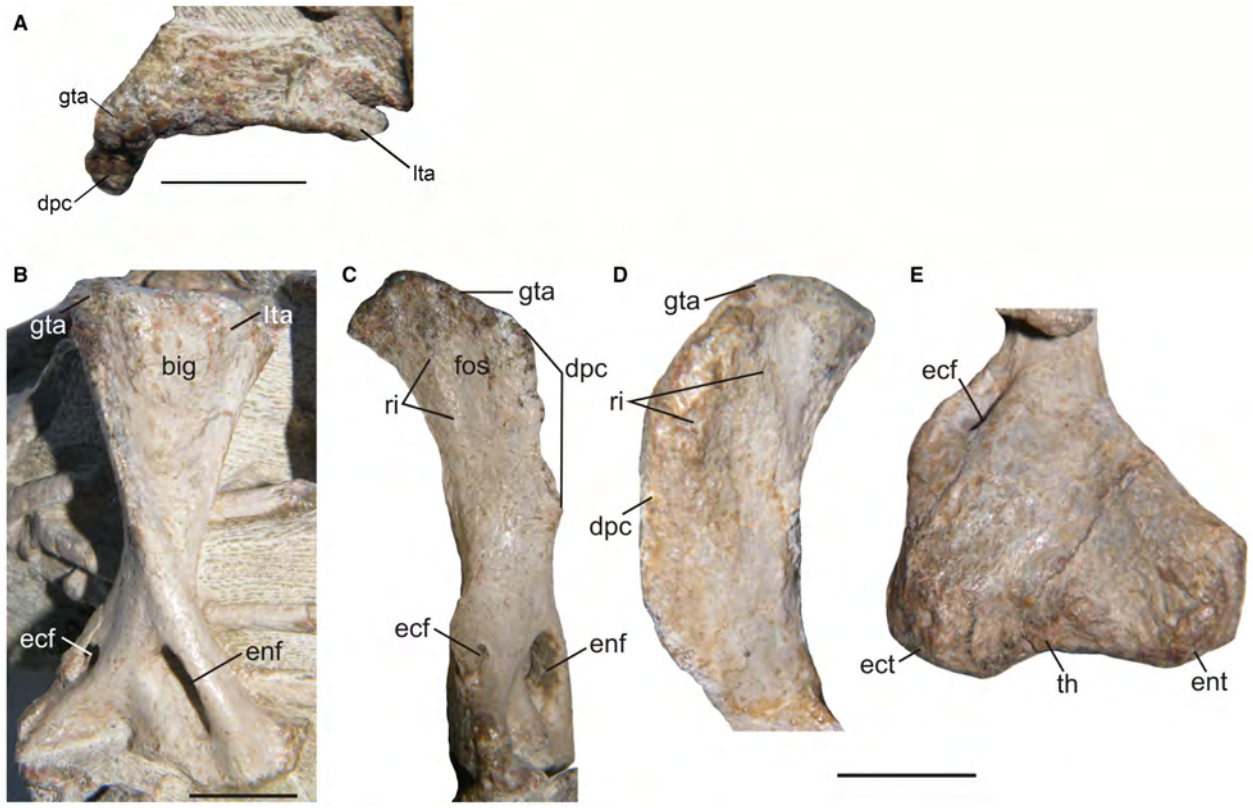


**FIG. 9.** Humerus of *Galesaurus planiceps*. A–B, NMQR 860, right humerus: A, ventral; B, lateral view. C–D, NMQR 3542 left humerus: C, lateral view of proximal and central portion; D, dorsal view of the distal portion. *Abbreviations*: big, bicipital groove; dpc, deltopectoral crest; ecf, ectepicondylar foramen; ect, ectepicondyle; enf, entepicondylar foramen; ent, entepicondyle; fos, fossa; gta, greater tuberosity area; lta, lesser tuberosity area; ri, ridge; th, trochlea. Scale bar represents 10 mm. Colour online.

row comprises the ulnare, intermedium and radiale, the second, two centralia and the third row has four distal carpals. A well-developed pisiform lies adjacent and proximal to the ulnare. The radiale and ulnare are the largest elements, whereas the first distal carpal is slightly smaller. The remaining bones of the carpus are clearly smaller than these three elements (Fig. 11B, C).

The pisiform, which articulates with the ulnare, is relatively flat with a rounded posterior and a slightly pointed anterior edge. The ulnare is flat, stout and almost rectangular (longer than wide) in shape. There is a small dorsal depression in the middle of the bone. It is thicker on the lateral side and slopes gently towards the thinner medial side. The dorsal surface of the ulnare is pitted and uneven, which may be due to poor ossification or preservation. The ulnare articulates with the intermedium and lateral centrale as well as the fourth distal carpal (Fig. 11B). In specimen SAM-PK-K10465, the medial and distal articulation facets of the ulnare are almost vertical. The intermedium is a small, irregular bone lying between the radiale and ulnare. The lateral side of the intermedium is convex and articulates with the ulnare, whereas the medial side is concave. The radiale is a stout, roughly oval, thick bone in dorsal view, wider than long, which tapers to a point proximolaterally (Fig. 11B, C). The dorsal surface of the radiale contains a rounded facet where it articulates with the radius, a wide lateral articulation with the lateral centrale as well as a wide, almost convex, articulation for the medial centrale. There is a medial, semicircular articulation facet on the radiale.

The two centralia are similar in size, the lateral centrale having unequal sides, with a wide articulation surface for the radiale and relatively smaller surfaces for the ulnare and the fourth distal carpal (Fig. 11B, C). The distal surface of the lateral centrale has a small central depression and a groove to which a muscle or ligament, active in manus movement, may have been attached. The medial centrale is wide and short in BP/1/4506 (Fig. 11C), and more quadrangular in SAM-PK-K10465 (Fig. 11B). The dorsal surface is round and smooth with a proximal facet for the radiale and distal facets for distal carpals 1 and 2.

Distal carpal 1 is a roughly quadrangular bone (Fig. 11B, C) that articulates with the sloping distomedial end of the lateral centrale, the large flat posterior end of metacarpal I and possibly with the small medial articulation surface of metacarpal II. All the articulation surfaces are almost vertical. The dorsal surface of the distal carpal is flat and pitted. The ventral surface of distal carpal 1 (SAM-PK-K10468; Fig. 11D) is indented and has a posteromedial tuberosity to which muscles or ligaments probably attached. Distal carpal 2, the smallest of the distal elements, is an almost rectangular bone lying posterior to metacarpal II (Fig. 11B, C). The dorsal surface is somewhat rounded with a slight anterior depression and thickens posteriorly. Distal carpal

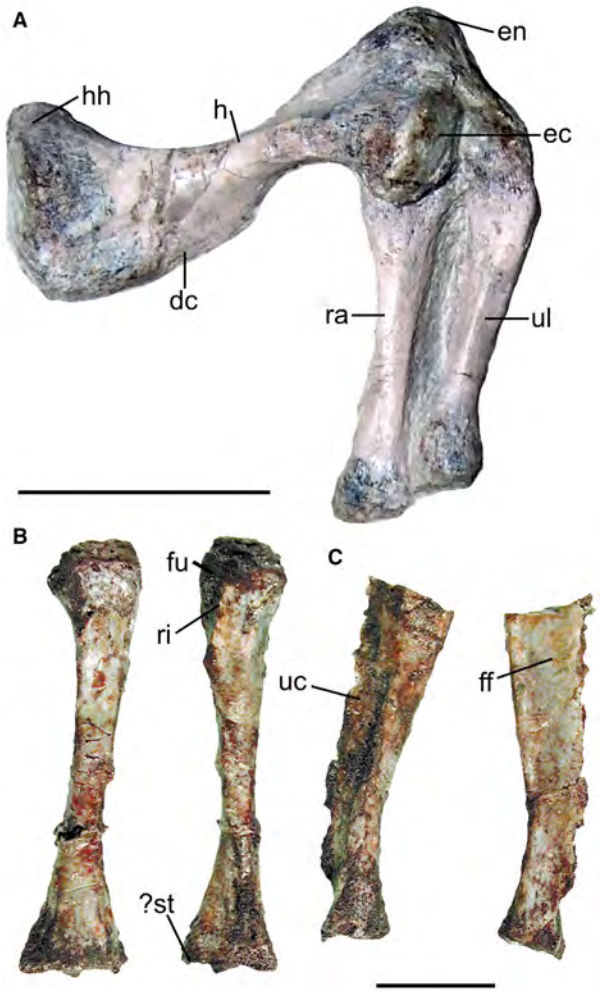


**FIG. 10.** Radius and ulna of *Galesaurus planiceps*. A, left humerus, radius and ulna of SAM-PK-K10465 in anterolateral view. B, left radius of SAM-PK-K1119 in anterior and posterior views. C, left ulna of SAM-PK-K1119 in lateral and medial views. *Abbreviations*: dc, deltopectoral crest; ec, ectepicondyle; en, entepicondyle; ff, shallow fossa for flexor muscles; fu, facet for articulation with the ulna; h, humerus; hh, humeral head; ra, radius; ri, ridge; ?st, ?styloid process; uc, ulnar crest; ul, ulna. Scale bars represent: 20 mm (A); 10 mm (B, C). Colour online.

3 is cylindrical and widens distally, where it articulates with the posterior end of metacarpal III (Fig. 11A–C). Distal carpal 4 articulates with the posterior end of metacarpal IV. The relative sizes of the distal carpals in SAM-PK-K10465 and BP/1/4506 are similar to those in *Thrinaxodon* (Jenkins 1971): I>IV>III>II (Fig. 11B, C).

In SAM-PK-K10465, the metacarpals are well-developed, robust bones. Robusticity, as an expression of bone width to length ratio, is notably prominent in metacarpals I to III, whereas the last two are more elongated, slender bones (Fig. 11B). Variation in metacarpal length is IV>III≈V>II>I, which is similar to that observed in most *Thrinaxodon* specimens. There is an interesting variation in BP/1/4506, where metacarpal I is longer than II and as long as metacarpal III (Fig. 11C). All the metacarpals are nearly symmetrical in dorsal view and have an elongated hourglass shape (Fig. 11B), whereas in ventral view, the bones are asymmetrical because the distal ends are thicker than the proximal ends (Fig. 11A). The square distal articulation facets are slightly convex in dorsal view, whereas the proximal ends have flat, almost rectangular articulation facets similar to those of *Thrinaxodon* (Jenkins 1971). The distal ends have uneven articulation surfaces that can be attributed to the presence of cartilage in life. On the proximal end, there is a mediolateral contact between adjacent metacarpals, apart from the first one. In the fourth metacarpal of subadult NMQR 3716, a clear line separates the diaphysis from the distal epiphysis (Fig. 11A).

The longest proximal phalanges are III and IV, with I and II slightly shorter and V the shortest. All the proximal phalanges have an hourglass shape with a similar expansion of the proximal and distal portions of the bone (Fig. 11A, B). Four tubercles, similar in size, can be seen in ventral view at the four 'corners' of the basal phalanges (Fig. 11A, D). Striations on the proximal and distal ends of the phalanges mark the attachments for ligaments or the M. flexor digitorum in a similar manner to that observed in ?*Cynognathus*/*Diademodon* (Jenkins 1971). A prominent feature is an anteroventral inclination of approximately 45° of the distal facet with respect to the long axis of the bone. The distal phalanges are only preserved in digits II and III. They are also hourglass-shaped, but the proximal ends are more expanded than the distal ends (Fig. 11A, B). Even where the manus of subadult SAM-PK-K10465 is completely preserved, it is clear that there are no reduced (disc-like) phalanges in digits II and III (Fig. 11B). In adult SAM-PK-K10468, digit III presents the classic mammalian formula of three phalanges, but the second phalanx is disc-like (Fig. 11D), whereas this reduced element is absent in digit II. In contrast, subadult NMQR 3716, has a disc-like phalanx in digit IV but none in digit III (Fig. 11A). A complete terminal phalanx in digit II is preserved in SAM-PK-K10465. It is similar in length to the distal (penultimate) phalanx and tapers to a sharp point (Fig. 11B).

The inferred phalangeal formula for SAM-PK-K10465 (lacking disc-like phalanges) is ?2-3-3-3-?3. In contrast, the presence of a disc-like phalanx in digit IV of NMQR 3716 followed by a non-ungueal phalanx indicates the putative presence of four phalanges in the digit. Finally, even when there is a disc-like phalanx in digit III of SAM-PK-K10468, the evidence shows that there were only three phalanges in the digit.

### *Posterior appendicular skeleton*

*Ilium.* This bone has a thin, expanded blade, separated from the acetabular region by a constricted neck (Fig. 12A, B). Facets for contact with the pubis and ischium, apart from that of the acetabulum, are present on the ventral portion. The iliac blade in the adult NMQR 3542 is well rounded and comparatively taller than in the subadults. The posterior lamina of the iliac blade has a slightly straighter posteroventral edge in the adult specimens, intersecting a moderately convex dorsal edge at approximately 80°. This lamina is comparatively longer and shallower towards its distal end in subadult RC 845. In

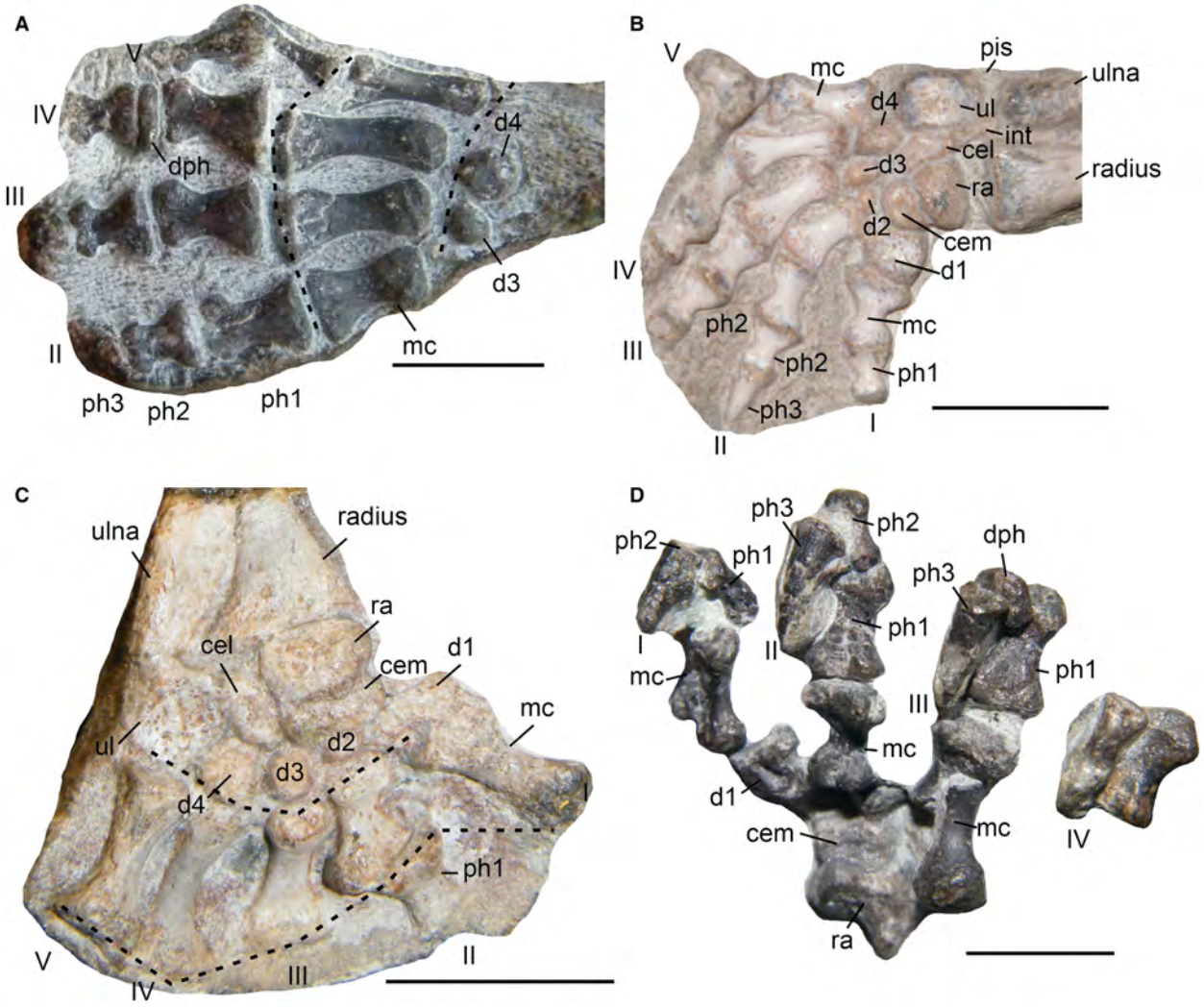


**FIG. 11.** Manus of *Galesaurus planiceps*. A, NMQR 3716, right manus ventral view. B, SAM-PK-K10465, right manus dorsal view. C, BP/1/4506, left manus ventral view. D, SAM-PK-K10468, left manus ventral view. *Abbreviations*: I–V, digits; cel, lateral centrale; cem, medial centrale; d1–4, distal carpals; dph, disc-like phalanx; int, intermedium; mc, metacarpals; ph1–3, phalanges; pis, pisiform; ra, radiale; ul, ulnare. Dotted lines connect proximal and distal margins of metacarpals and phalanges. All scale bars represent 2 mm. Colour online.

*Thrinaxodon* and subadult *Galesaurus*, the dorsal edge of the iliac blade is less convex (Fig. 12A). The posterior and dorsal margins of the iliac blade taper to form a sharp rim (Fig. 12B). Prominent striations were observed along these margins in lateral view in adult NMQR 3542. The medial surface of the iliac blade of this specimen is uneven, showing striations on the rugose dorsal edge that possibly represents the presence of connective tissue for the sacro-iliac fusion (Jenkins 1971). Striations on the posterior surface of the iliac blade are not visible due to the position in which the ilium is preserved. The iliac blade of subadult *Galesaurus* exhibits smaller and roughly evenly spaced striations on the medial and dorsal surfaces, whereas the posterior surface has a few horizontal striations just above the posteroventral edge (Fig. 12B). The anterior portion of the iliac blade of subadult RC 845 has a distinct, shallow depression directed dorsoventrally and obliquely towards the supra-acetabular buttress (Fig. 12B). A laterally projecting supra-acetabular buttress, an anteroventrally-directed process for the articulation with the pubis and a posteroventrally-directed process for the ischium are present on the inferior margin of the ilium of subadult RC 845 (Fig. 12B). The lateral rim of the buttress is round whereas the facet itself is concave and faces ventrally. A supra-acetabular notch lies posterior to the buttress. The facets for the pubis and ischium, clearly exposed in RC 845, are strap-shaped and widen towards the anterior (pubic) and posterior (ischial) ends. The pubic facet is more than half the length of the ischial facet. The posterior portion of the ilium, in both subadults and adults, extends to form a distinct, elongated projection.

*Pubis.* The pubis is formed by the laterally concave pubic plate (Fig. 12C), which is directed ventromedially and represents two-

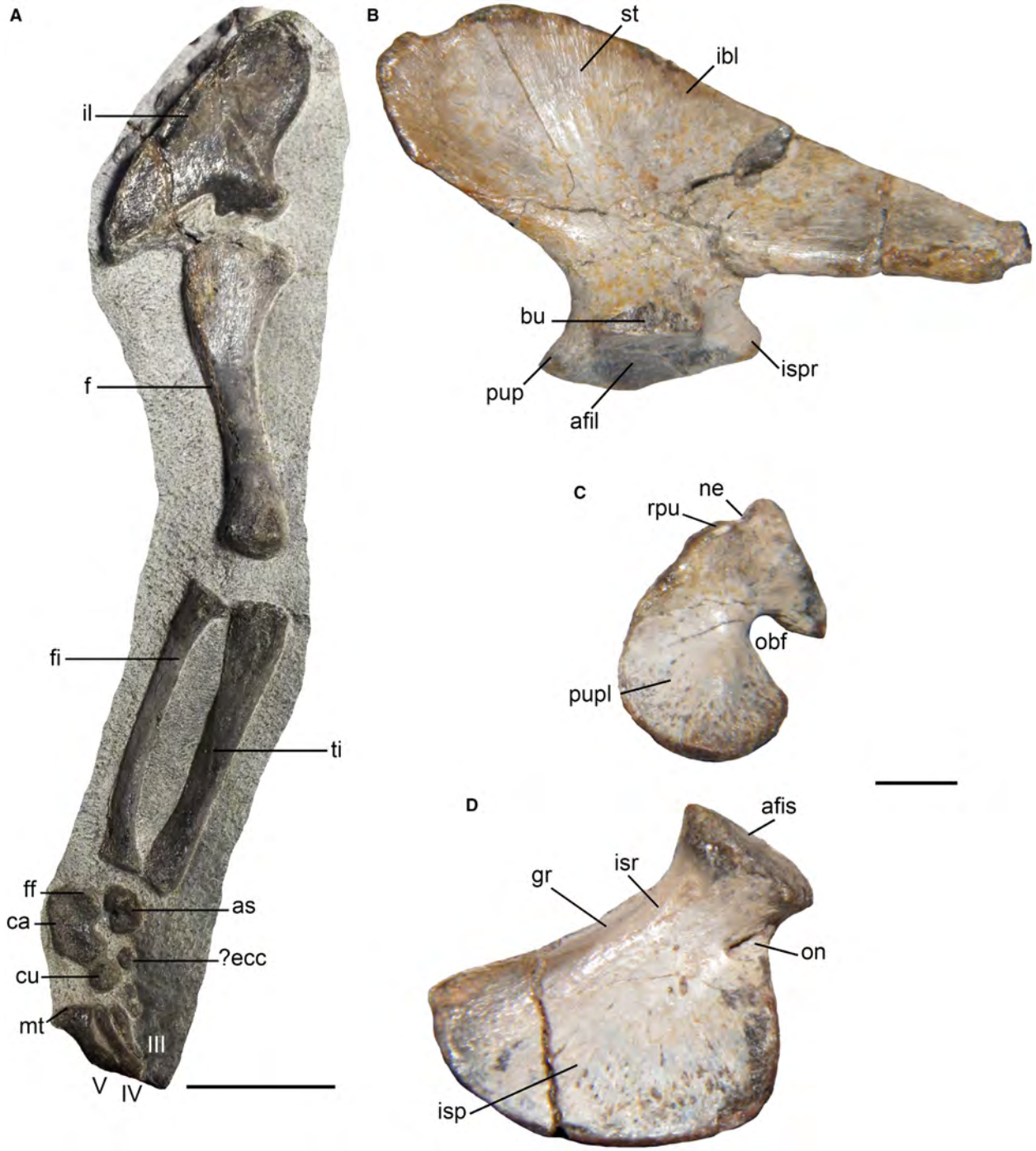


**FIG. 12.** Pelvis of *Galesaurus planiceps*. A, right ilium and posterior limb NMQR 3716. B, left ilium of RC 845 in lateral view. C, left pubis of RC 845, in lateral view. D, right ischium of RC 845. *Abbreviations*: III–V, digits; afil, acetabular facet of the ilium; afis, acetabular facet of the ischium; as, astragalus; bu, supra-acetabular buttress; ca, calcaneum; cu, cuboid; ?ecc, ?ectocuneiform; f, femur; ff, fibular facet; fi, fibula; gr, groove; ibl, iliac blade; il, ilium; isp; ischial plate; ispr, ischial process; isr, ischial ridge; mt, metatarsal; ne, neck; obf, obturator foramen; on, obturator notch; pup, pubic process; pupl, pubic plate; rpu, rod-like anterodorsal edge of pubis; st, striations; ti, tibia. Scale bars represent: 20 mm (A); 5 mm (B–D). Colour online.

thirds of the ischial plate. The acetabular facet is oval and flat. Jenkins (1971) suggested that the cartilaginous articulation surface in cynodonts was probably concave during life and this was probably also the case in *Galesaurus*. The facet of the pubis is the smallest facet forming the acetabulum. Just below the acetabular facet, the pubis constricts to form a short neck (Fig. 12C),

which is more elongated in the ontogenetically older specimens. Following the neck, the anterior margin of the pubis produces a rod-like structure ending in a rounded rugosity, which is incipient in subadult (Fig. 12C) and well-developed in adult individuals. The anterior edge of the pubic plate appears to be complete and is relatively uneven indicating that cartilage may have been present. In subadult RC 845, the obturator foramen is notably small and represents one-third of the pubic plate.

*Ischium.* The acetabular facet is quadrangular, with an almost straight medial border and appears to be flat in subadult RC 845 (Fig. 12D). In adult NMQR 3542, the facet is oriented anterolaterally and slightly dorsally. The ischial plate in RC 845 is relatively thin and subtriangular whereas in NMQR 3542 it is more robust and thicker. In the subadult individuals it is anteroposteriorly elongated (Fig. 12D), slightly concave laterally and deeply concave medially. The ischium of RC 845 has a tiny notch on the anterior margin of the plate that represents the posterior margin of the obturator foramen; the foramen is thus remarkably smaller than that of the pubis. The anterior margin of the plate, below the acetabular notch, is thicker than the posterior margin, slightly laterally-oriented, and produces the lateral concavity of the plate that ends dorsally with the ischial ridges (Fig. 12D). A fairly pronounced ischial ridge extends from the posterior portion of the acetabular rim on the ischial head to three-quarters of the way towards the posterodorsal corner of the ischial plate in RC 845. This rim is more developed in NMQR 3542. In both specimens, a second more elevated and conspicuous ridge is located on the dorsomedial margin of the bone, whereas a shallow groove, with a wide proximal area is present between these ridges (Fig. 12D). This groove is well-developed in adult specimens, which would indicate its function as a point of muscle origin. The ischial tuberosity, a distinct lateral thickening of the mediolateral ischial plate, is present on the dorsoposterior margin of the ischium.

*Femur.* The femur is a robust bone (Fig. 13). The head of the femur is slightly swollen and oval in outline (Fig. 13A, C–F). The articulation surface has a rough texture from the head to the greater trochanter, which probably indicates the presence of a cartilaginous cap that articulated with the pelvic girdle. This region is considerably thicker in the subadults compared to the adults. The proximal portion of the femur is directed dorsally and shows an angulation between 30 and 35 degrees with respect to the long axis of the bone (Fig. 13C–F). The greater trochanter (Fig. 13A, D, F) is enlarged and expanded laterally. In *Thrinaxodon* and subadult *Galesaurus*, the greater trochanter is slightly thicker than the connecting ridge to the head (Jenkins 1971, fig. 13A). This is in contrast to ontogenetically older *Galesaurus* where the greater trochanter expands dorsally and is as thick as the connecting ridge. Two surfaces can be distinguished on the greater trochanter; one facing dorsally and the other ventrally. Jenkins (1971) interpreted the first as the probable insertion area for M. ischio-trochantericus (= M. obturator internus and gemelli of extant mammals) and the ventral area as the attachment for M. ilio-femoralis (= M. gluteus of extant mammals). We consider the gluteal muscles to have attached to both dorsal and ventral surfaces of the greater trochanter (Evans 1993) because the M. obturator externus, M. obturator internus and M. gemelli in extant mammals are usually attached to the intertrochanteric fossa (Evans 1993; Oliveira 2010).

An even, shallow concavity is present on the dorsal surface of the proximal end situated just below the femoral head and greater trochanter. It probably represents the origin for part of the M. femoro-tibialis (= M. vastus of mammals; Jenkins 1971,


**FIG. 13.** *Galesaurus planiceps*, right femur of NMQR 3542 (cast). A, proximal; B, distal; C, dorsal; D, ventral; E, medial and F, lateral views. *Abbreviations*: fh, femoral head; ft, shallow depression for attachment of the M. femorotibialis; gr, groove; gtr, greater trochanter; if, intertrochanteric fossa; lc, lateral condyle; ltr, lesser trochanter; mc, medial condyle, se, sediment covering the bone. Scale bar represents 10 mm. Colour online.

fig. 13E). This concavity gradually tapers distally and ends ventral to the midshaft.

Both subadult and adult *Galesaurus* have a round, deep intertrochanteric fossa between the lesser and greater trochanters (Fig. 13D). Jenkins (1971) interpreted the attachment of M. pubo-ischio-femoralis externus in this fossa as extending to the proximal end of the trochanteric crest and into the lesser trochanter, with no evidence that the attachment extended distally along the crest (Jenkins 1971).

The lesser trochanter of adult *Galesaurus* is a prominent bone extension that begins distal to the femoral head and runs along the shaft. The trochanteric crest, following the lesser trochanter, is incipient and ends just above the midpoint of the shaft. As noted by Haughton (1924) and Broom (1932*a*), the crest continues as a sharp border to the distal medial condyle (Fig. 13D), a condition also present in *Thrinaxodon* (Jenkins 1971). There is no third trochanter in *Galesaurus*. In the eucynodonts *Diademodon* and *Cynognathus*, the anterior and ventral surfaces distal to the lesser trochanter meet in a short groove (Jenkins 1971; fig. 13D). In subadult *Galesaurus*, this groove is more prominent than in the adult specimens. A long, shallow groove occurs where the distal surface of the lesser trochanter meets the femoral shaft in anteromedial view, and probably represents the insertion for M. pubo-ischio-femoralis internus (Jenkins 1971). In ventral view, a broad fossa on the lesser trochanter tapers gradually towards the distal end.

This study confirms Broom's (1932*a*) initial observation that the lateral and ventral surfaces of the femoral shaft in *Galesaurus* are separated by a rounded crest that runs from the greater trochanter to the midshaft (Fig. 13F). This is in contrast to *Cynognathus* and *Diademodon* where the crest is more angular and runs from the greater trochanter to the side of the lateral condyle (Jenkins 1971). The femoral shaft of *Galesaurus* is roughly square in cross-section through the midshaft and expands lateromedially to become more rectangular further down the shaft. Parts of the M. femoro-tibialis probably originated on the dorsal surface as well as the medial and lateral areas of the expanded distal portion.

The lateral condyle is clearly larger than the medial condyle in the adult NMQR 3542 (Fig. 13B). An incipient ridge connects the two condyles in ventral view. It forms the lower border of a triangular depression, which is located on the distal third of the bone, limited laterodistally by the condyles (Fig. 13D). The distal condyles of the femur have a rough and uneven texture, which probably indicates the presence of a cartilaginous cap that articulated with the tibia.

*Tibia.* The expanded proximal surface of the tibia is asymmetrical because of the projection of the lateral condyle (Fig. 14A). The condyle, which articulates with the fibula, has a convex medial margin, but a distinct rounded, laterally-oriented projection. It is followed by a blunt ridge that borders a fossa (sulcus extensorius) posteriorly and the cnemial crest anteriorly. This fossa was probably for the origin of the M. tibialis cranialis (to flex the tarsus and rotate the paw laterally; Evans 1993). The anterodorsal portion of the tibia has an incipient cnemial crest in both the subadults (RC 845) and adults (NMQR 3542). In RC 845, longitudinal striations on the surface of the cnemial crest indicate the probable attachment of the M. biceps femoris, which ends close to the proximal third of the bone (Fig. 14A). A second, smaller fossa is located behind the rounded ridge and the posterior margin of the bone. This area is a possible site for the origin of the M. flexor hallucis (digit I) longus. The lateral face of the proximal third of the tibia has a few striations again indicating an area of muscle attachment. In contrast, the middle portion of the bone is smooth. The tibial shaft flattens laterome-dially and is concave proximally, straightening towards the distal portion of the posterior margin. The distal end of the bone is laterodistally expanded, but far less so than the proximal portion. The distal surface of the tibia in adult NMQR 3542 is quadrangular.

*Fibula.* The fibula is an elongated bone with a slender shaft that expands slightly at each end, with the proximal end being

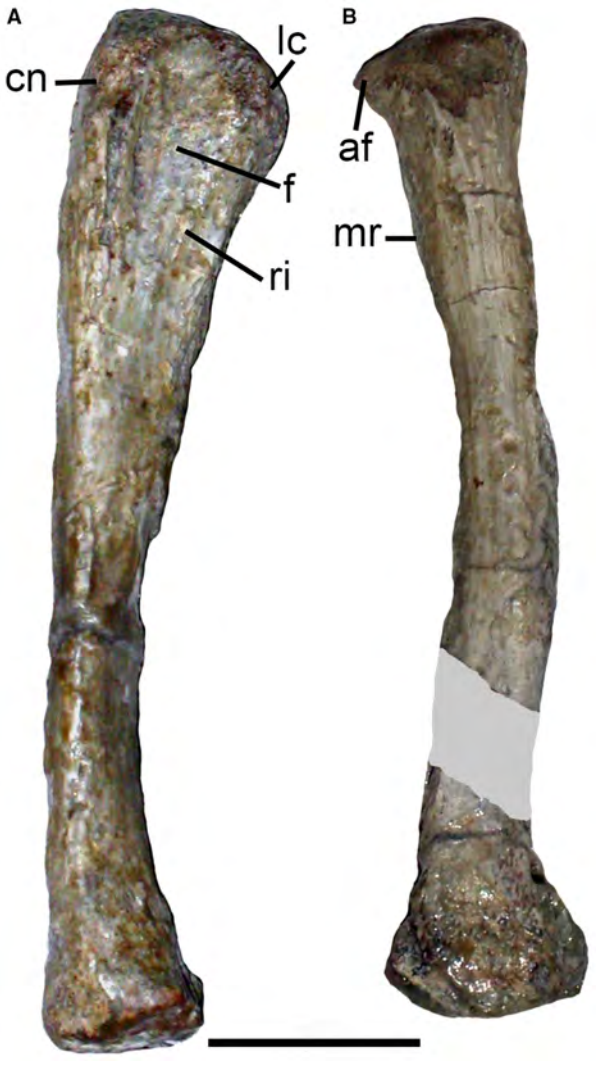


**FIG. 14.** *Galesaurus planiceps*, NMQR 3542. A, left tibia. B, left fibula; grey area indicates the portion of the fibula covered by the tibia and is not visible. *Abbreviations*: af, articulation for femur; cn, cnemial crest; f, fossa; lc, lateral condyle; mr, medial ridge; ri, ridge. Scale bar represents 10 mm. Colour online.

slightly broader than the distal end. Only the proximal end in subadult RC 845 is preserved, but it is not as expanded as it is in adult NMQR 3542 (Fig. 14B). The articulation surfaces face medially and slightly dorsally, with the proximal end being rounded and slightly convex. There is a prominent flange in the anteroproximal corner of the fibula (Fig. 14B). This may have been part of the articulation between the femur and fibula, but perhaps served as a musculotendinous process (Jenkins 1971). The shaft appears triangular in cross-section.

The fibula of the adult specimens corresponds to fibular type II in *Thrinaxodon* (Jenkins 1971) described as a bone with a sharp ridge descending from the proximal end along the medial side and continuing with a second ridge down the posteromedial side. As in *Thrinaxodon*, a longitudinal groove is present on the medial surface of the fibula (Jenkins 1971) in both subadult and adult specimens. However, the distal end of the fibula in *Galesaurus* is almost oval in cross-section, which is in contrast to the triangular cross-section described for *Thrinaxodon* (Jenkins 1971).

*Pes.* In the pes of the adult BP/1/4506 it is possible to recognize five tarsal bones, five metatarsals, one complete phalanx in digits I, IV and V, and two complete phalanges in the remaining two digits (Fig. 15). Following our interpretation of the tarsal bones, the entocuneiform is the largest distal element and is a robust quadrangular bone articulating with metatarsal I distally and the navicular bone proximally. Part of the lateral side of the entocuneiform is in contact with the medial side of metatarsal II (Fig. 15). The ectocuneiform is partially covered by the navicular, but is clearly much smaller than the entocuneiform. The navicular has an irregular elliptical form with a central dorsal fossa. It has been displaced and thus, its specific orientation and articulation with the distal tarsal is unknown. The cuboid is irregularly shaped and contacts metatarsal IV distally and metatarsal III just slightly (Fig. 15). It contacts a round bone proximally, which we interpret as the astragalus. Although partially covered by the navicular, it is clearly the largest tarsal bone. The dorsal surface of the astragalus is pitted and uneven. The partial pes of subadult NMQR 3716 (Fig. 12A) includes an enormous rectangular calcaneus, showing a notch on the medial side, towards the astragalus, which represents the calcaneal sulcus. The tubercle, situated on the posterolateral margin of the calcaneum, was not observed in this specimen. A rounded surface posterior to the sulcus is interpreted as the fibular facet (Fig. 12A). The astragalus is quadrangular, showing a medial bulbous surface as in the case of the unidentified Middle Triassic cynodont from the Manda Formation (Jenkins 1971, fig. 60). There is a notch on the lateral side of the astragalus (Fig. 12A) that probably represents the origin of the astragalar sulcus. A subrectangular cuboid contacts the proximomedial margin of the calcaneus. This bone is half the size of the astragalus. The smallest preserved tarsal bone is located medial to the cuboid and anterior to the proximal margin of the astragalus (Fig. 12A). Considering the size of this element, we identify this bone as the ectocuneiform.

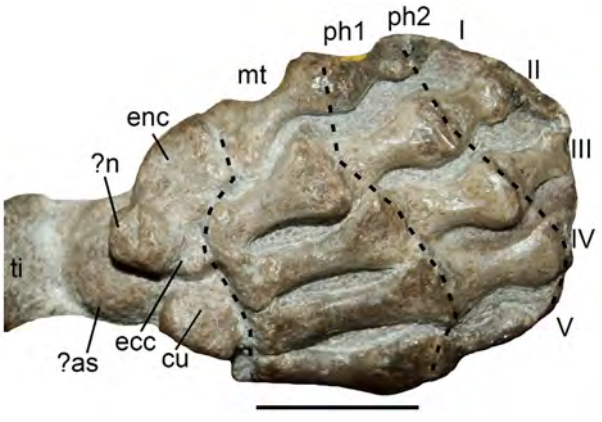


**FIG. 15.** *Galesaurus planiceps*, right pes of BP/1/4506 in dorsal view. Dotted lines connect proximal and distal margins of metatarsals and phalanges. *Abbreviations*: I–V, digits; ?as, ?astragalum; cu, cuboid; ecc, ectocuneiform; enc, entocuneiform; mt, metatarsals; ?n, ?navicular; ph1–2, phalanx 1–2; ti, tibia. Scale bar represents 10 mm. Colour online.

In BP/1/4506, metatarsals I, III, IV and V are more slender than metatarsal II (Fig. 15). The relative lengths of the metatarsals are IV>III>V> (I = II). The distal end of each metatarsal flares laterally and more so than the proximal end. All the metatarsals have an almost lateromedially symmetrical, elongated hourglass shape. The proximal portion of metatarsal I is more distally located than the remaining metatarsals because of the position of the entocuneiform (Fig. 15). The distal end of this metatarsal is more distally located than the distal end of metatarsal II, but at the same level as the distal ends of metatarsals III–V.

All the proximal phalanges, except the fifth, are completely preserved. They are similar in shape to, but slightly shorter than, the metatarsals. The proximal ends are smooth and thus, do not suggest extensive cartilage coverage during life. The proximal and distal ends are almost equal in width. The proximal phalanges of digits III and IV are longer than those of digits I and II (with digit I being the shortest). The central phalanges are only preserved in digits II and III. They are quadrangular, hourglass shaped and shorter than the proximal phalanges. The central phalanx of digit III is slightly more robust than that of digit II. None of the terminal phalanges of any specimen are preserved. There is a reduced disc-like phalanx in digit IV and thus, the available material suggests that the digital formula of the *Galesaurus* pes is 2-?3-?3-?4-?3.

### *Osteohistology*

The tibia and fibula of RC 845 (63% adult) contain rapidly growing bone tissues (Fig. 16A–D). The numerous, large, round osteocyte lacunae are haphazardly arranged in a woven-fibred bone matrix. The vascular canals (tibia 3.2%; fibula 6%) comprise longitudinally-oriented primary osteons in radial rows or radiating primary osteons that extend to the sub-periosteal surface. These features represent rapidly forming fibro-lamellar bone. The medullary cavity is open and devoid of bony trabeculae in both bones. Secondary remodelling is restricted to a small patch in the tibia, which contains a few tiny secondary osteons

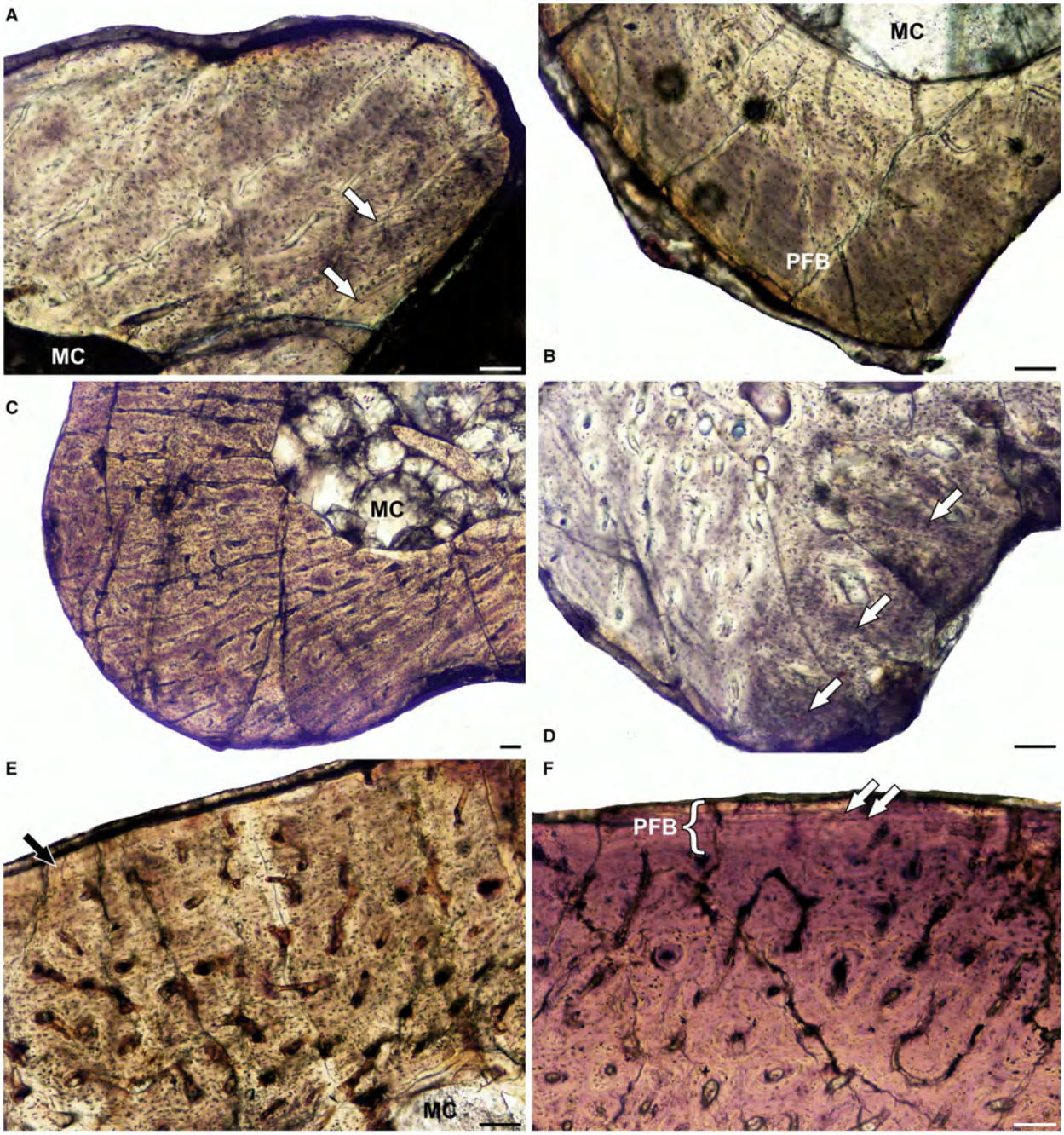


**FIG. 16.** Limb bone osteohistology of *Galesaurus planiceps*. A, RC 845 tibia showing radiating vascular canals and Sharpey's fibres (arrows). B, RC 845 tibia showing a region of parallel-fibred bone. C, RC 845 fibula showing highly vascularized radiating fibro-lamellar bone. D, RC 845 fibula showing prominent Sharpey's fibres (arrows). E, NMQR 135 humerus showing highly vascularized fibro-lamellar bone; arrow indicates the onset of a parallel-fibred bone region. F, NMQR 3716 femur showing highly vascularized fibro-lamellar bone; arrow shows the onset of a region of parallel-fibred bone at the periphery. *Abbreviations*: MC, medullary cavity; PFB, parallel-fibred bone. All scale bars represent 100 μm.

and a layer of secondary endosteal bone lining the medullary cavity. A few relatively large resorption cavities are present on the posteromedial side of the fibula. A layer of circumferential endosteal tissue is also restricted to small areas, the rest of the peri-medullary region being exposed, showing that growth was still active. There is no decrease in growth rate in the fibula and most of the tibia, supporting the hypothesis that the smaller, gracile morphs represent ontogenetically younger individuals that were still actively growing at the time of death (RC 845) (Butler 2009). However, there is a region on the posterior side

of the tibia that reveals slower growing bone with fewer, simple radiating canals. Here, the osteocyte lacunae remain globular as in the fibro-lamellar region, but they are smaller and fewer in number. They are randomly distributed throughout this region, but lamellae running parallel to one another can clearly be seen indicating the presence of parallel-fibred bone (Fig. 16B). These features indicate that, although still actively growing at the time of death, parts of the bone had begun to grow more slowly, suggesting that the subadult stage had been reached. This interpretation supports the calculated percentage adult size of 63%, indicating that RC 845 was a subadult and not a juvenile. Growth marks in the form of annuli (representing a temporary decrease in growth) or lines of arrested growth (LAGs; representing a temporary cessation in growth; Francillon-Vieillot *et al.* 1990) are absent from both elements.

Sharpey's fibres, indicating areas of muscle and ligament attachment (Francillon-Vieillot *et al.* 1990), were observed in both elements (Fig. 16A, D, arrows). In the fibula, they form a deep, prominent bundle of fibres indicating the insertion of a muscle of uncertain origin.

The humerus of NMQR 135 (65% adult) is almost complete apart from a missing medial fragment of the midshaft. Part of the medullary cavity and the compact cortex of the medial side of the bone in the midshaft sections are missing, but the rest of the bone is well preserved allowing the structure of the bone tissue to be clearly seen. The bone contains relatively highly vascularized (7.7%) fibro-lamellar bone with large osteocyte lacunae and vascular canals scattered randomly throughout the cortex (Fig. 16E). These canals are a mixture of longitudinally-oriented simple canals, but mostly primary osteons with a few short anastomoses. They become more radial in the region of the deltopectoral crest and the dorsolateral corner of the bone. These areas probably represent areas of muscle attachment. There is no general decline in vascularization towards the bone periphery, but a thin layer of avascular parallel-fibred bone at the sub-periosteal surface was observed in one small region on the dorsal side of the bone. The rest of the bone shows clear signs of continued active growth. Growth marks are absent, although the possibility of the small outer region of lamellar bone representing a growth mark cannot be ruled out. However, the region may equally represent the onset of an overall transition to slower forming bone tissues. If so, however, this individual was still relatively young at the time of death as the deposition of slowly forming tissue, usually indicating some form of maturity (skeletal or reproductive) had only just begun (West *et al.* 2001).

Femur NMQR 3716 (71% adult) comprises moderately vascularized (5%) fibro-lamellar bone (Fig. 16F). Abundant globular osteocyte lacunae are haphazardly arranged in a woven-fibred bone matrix. Longitudinally-oriented primary osteons are predominantly arranged in radial rows, with some radiating out to the sub-periosteal surface (although not as much as in RC 845). Growth marks are absent from the mid-cortex. However, a LAG (which appears double in some areas) was observed in the outermost cortex. The bone tissue in this region transforms into slowly forming, mostly parallel-fibred bone. Here, a mixture of rounded and flattened osteocyte lacunae are arranged either randomly or in parallel rows, and the vascular canals are generally simple, short, radiating channels. A few bony trabeculae extend into an otherwise open medullary cavity. A relatively thin layer of endosteal circumferential bone borders the medullary cavity in some places, but resorption was clearly active with several resorption cavities in the peri-medullary region. The bone tissue in NMQR 3716 supports the hypothesis that this robust morph represents an ontogenetically older individual.

The osteohistology of several elements of NMQR 3542 was available for study (Fig. 17). The bone tissues of all the elements comprise fibro-lamellar bone in the inner and mid-cortex with a transition to slower lamellar-zonal bone in the outer cortex. The slow growing tissue is similar to that seen in the other specimens, i.e. a mixture of globular and flattened osteocyte lacunae either randomly distributed or arranged in parallel, and clear lamellae running parallel to one another. The humerus contains a notably small medullary cavity with small to large resorption cavities lined with thick layers of endosteal lamellae. The bone tissue contains predominantly longitudinally-oriented primary osteons with a few short anastomoses scattered throughout the inner and mid-cortex. Vascularization is moderate (4.6%), decreasing further within the peripheral lamellar-zonal bone tissue (Fig. 17A). A LAG was observed at the periphery, but multiple, closely spaced LAGs indicating an external fundamental system (EFS) are absent. An EFS indicates that an individual has reached full adult size and has essentially stopped growing (Cormack 1987).

The radius of NMQR 3542 has a notably thick cortex and a tiny medullary cavity, which is lined by thick layers of circumferential endosteal lamellae (Fig. 17B). The bone tissue is similar to the humerus with fibro-lamellar bone in the inner and mid-cortex and a transition in the outer third to parallel-fibred, but predominantly lamellar-zonal bone. However, the slower growing region is thicker than that of the humerus. The vascular canals are either longitudinally-oriented primary osteons in radial rows or radiating canals (1.7%) with a decrease in vascularization in the outer lamellar bone to mostly simple canals. Secondary remodelling is limited to the peri-medullary region in the form of a few resorption cavities and tiny secondary osteons. A single LAG was observed in the outer periphery, similar to the humerus (Fig. 17B). Sharpey's fibres were observed on the posteromedial side of the bone indicating the possible insertion of the M. biceps.

The ulna has a thick cortex similar to the radius. A few bony trabeculae traverse the small main medullary cavity and there are a few large resorption cavities in the peri-medullary region. The cortex contains relatively poorly vascularized (2.5%) fibro-lamellar bone with predominantly longitudinally-oriented primary osteons throughout the inner and mid-cortex. The canals are more radially oriented in the area of the ulnar crest. The outermost cortex contains poorly vascularized lamellar-zonal bone with a LAG, but the region is thinner than that seen in the radius. Prominent Sharpey's fibres (Fig. 17C) were observed on the lateral side of the ulnar crest for the possible attachment of the radio-ulnar interosseous ligament and on the posterior side of the bone for the possible attachment of the flexor muscles (Jenkins 1971).

The femur of NMQR 3542 has a thinner cortex compared to those of the forelimb, with numerous resorption cavities having resorbed the innermost cortex. The inner and mid-cortex

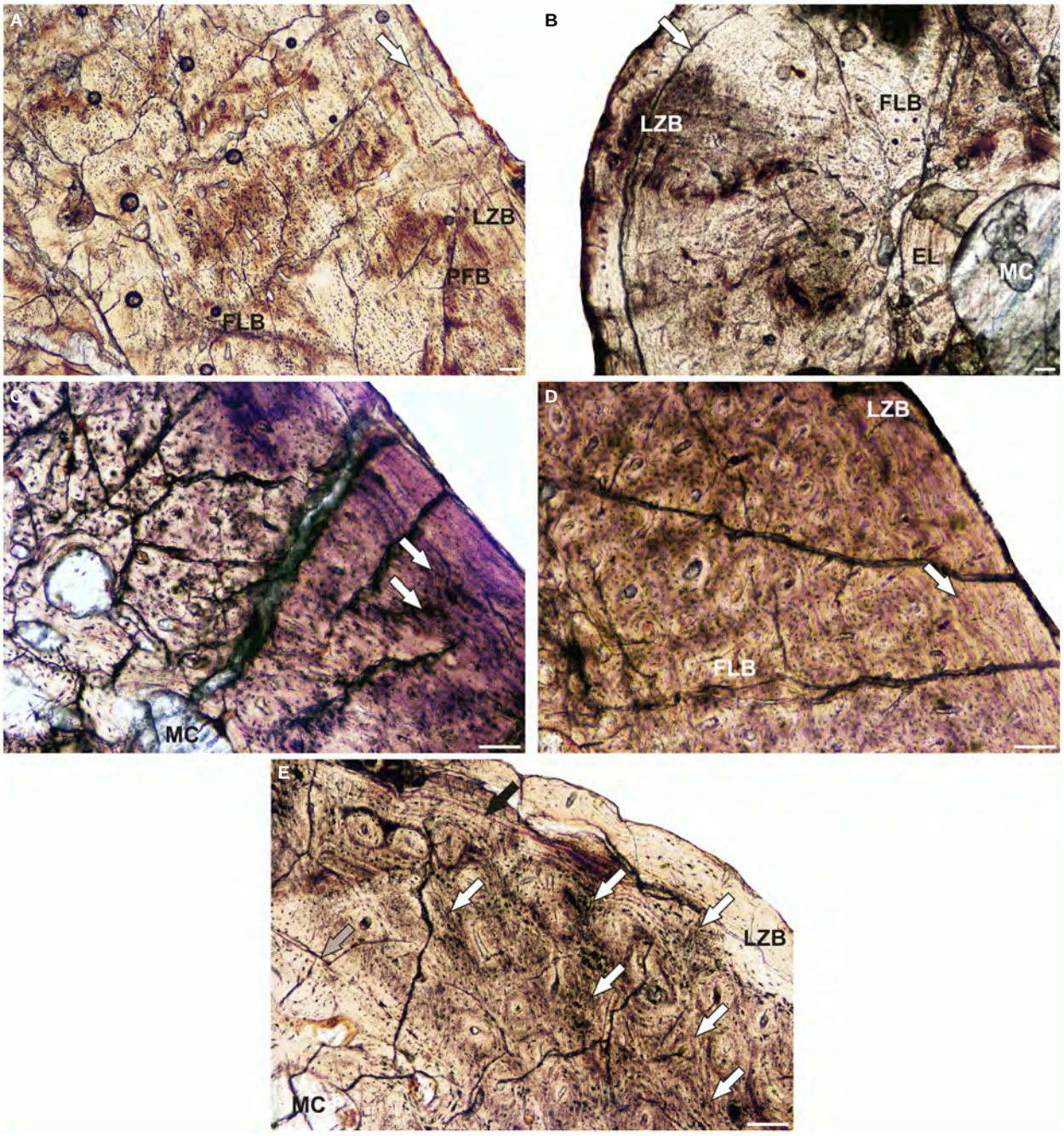


**FIG. 17.** Limb bone osteohistology of *Galesaurus planiceps* NMQR 3542. A, humerus showing a transition from fibro-lamellar bone to parallel-fibred bone to peripheral lamellar-zonal bone; arrow represents a LAG. B, radius showing a thick cortex of inner fibro-lamellar bone becoming lamellar-zonal bone towards the periphery; arrow indicates a LAG. C, ulna showing prominent Sharpey's fibres (arrows). D, femur showing transition from fibro-lamellar bone to peripheral lamellar-zonal bone; arrow represents a LAG. E, tibia showing a LAG (black arrow) within the peripheral lamellar-zonal bone and numerous Sharpey's fibres (white arrows); grey arrow indicates a reversal line. *Abbreviations*: EL, endosteal lamellae; FLB, fibro-lamellar bone; MC, medullary cavity; PFB, parallel-fibred bone; LZB, lamellar-zonal bone. Scale bars represent 100 μm.

contains moderately vascularized (4.8%) fibro-lamellar bone (Fig. 17D). The vascular canals are a mixture of longitudinally-oriented primary osteons and short radial canals that are randomly distributed throughout the cortex. The slower forming peripheral bone tissue consists of lamellar-zonal bone and contains a single LAG, similar to that seen in the other elements of NMQR 3542. There are fewer, simple vascular canals in this region.

The fibro-lamellar bone of tibia NMQR 3542 contains relatively few longitudinally-oriented primary osteons either randomly distributed or arranged in radial rows (2.7% vascularization). The medullary cavity is largely open, but there are numerous bony trabeculae in the peri-medullary region. The trabeculae are lined with several layers of endosteal lamellae and a reversal line is visible in one section on the posterolateral side of the bone (Fig. 17E). The slower growing peripheral region has fewer vascular canals, randomly distributed osteocyte lacunae and clear lamellae. A LAG runs through the outermost cortex. Prominent Sharpey's fibres were observed on the posterolateral side of the bone for the insertion of flexor muscles (Fig. 17E).

The microanatomy of the forelimb elements of *Galesaurus* was also assessed. The largest, adult individual (NMQR 3542) was used to obtain the global compactness (Cg), which estimates the overall compactness of the cortex, and K, which estimates the thickness of the cortical bone. The microanatomy of the humerus, radius and ulna of NMQR 3542 revealed compact cortices and relatively similar values between the bones (humerus Cg = 0.945; radius Cg = 0.946; ulna Cg = 0.958). The cortical thickness values are also relatively similar between the elements and all reveal a notably thick cortex (humerus $K = 0.13$; radius $K = 0.23$; ulna $K = 0.14$). The femur and tibia of NMQR 3542 were also assessed and revealed slightly lower Cg values of 0.846 and 0.838, respectively. The $K$ values revealed thinner cortices compared to the forelimb with 0.42 for the femur and 0.43 for the tibia.

## DISCUSSION

### *Postcranial variation of* Galesaurus *through ontogeny*

The examination of the material in this study reveals the presence of two distinct morphs, namely a small, gracile, and a large, robust form. We consider the two morphs to represent different stages within an ontogenetic series, with the small morph representing juveniles and subadults (BSL < 90 mm) and the large morph, adults (BSL ≥ 90 mm) (see also Jasinoski & Abdala 2017*a*). Variation in the skulls of the adults includes the presence of a suborbital angulation between the jugal and maxilla (Abdala 2003; Abdala & Damiani 2004; Jasinoski & Abdala 2017*a*). Interestingly, the skull morphology of the subadult specimens resembles that of *Thrinaxodon*, whereas the angulation between the jugal and maxilla mentioned above in the adults is typical of the Late Triassic carnivorous cynodont *Chiniquodon* (Abdala & Giannini 2002), and is only represented in two large specimens of *Thrinaxodon* (e.g. Jasinoski *et al.* 2015).

The axial skeleton of the two morphs is similar, but because nearly all the well-preserved axial skeletons in our sample are articulated and only partially visible, differences between them cannot be ruled out. There are three subadults with articulated axial skeletons where the full number of presacral vertebrae can be counted. Two specimens, BP/1/4506 and SAM-PK-K10465, have 29 presacrals (Fig. 1), whereas RC 845 has 25 (Figs 2, 3). The count in the latter specimen, however, is tentative because the two blocks containing the skeleton do not fit well and it is possible that more vertebral elements were present in life. A variation of 26–28 presacrals is observed in *Thrinaxodon* (Müller *et al.* 2010; FA pers. obs.), whereas 25–29 presacral vertebrae is the general range in most non-mammaliaform synapsids in which the presacral count is known (Müller *et al.* 2010, supplementary information). The cynodont *Trucidocynodon* is a notable exception with the inordinate count of 32 presacrals (Oliveira *et al.* 2010). Narita & Kuratani (2005) proposed a count of 19 thoracolumbar vertebrae as representative of mammals (i.e. monotremes, marsupials, several placentals and the 125 million year old eutherian *Eomaia*). The thoracolumbar number in *Galesaurus* varies between 18 and 22 and the counts in other cynodonts range from 19 (*Massetognathus*) to 22 vertebrae (Müller *et al.* 2010). Considering the variation in the thoracolumbar vertebral formula, there is no evidence in Permo-Triassic cynodonts of the developmental constraints that had an important effect on the vertebral count of extant mammals (Narita & Kuratani 2005). The difference in the number of presacrals between *Galesaurus* specimens RC 845 and SAM-PK-K10465 is probably due to the different thoracic vertebral counts (?11 vs 15). The number of presacral vertebrae recognized in *Galesaurus* (?25 to 29 elements) is commonly represented in extant mammals (Narita & Kuratani 2005, table 1; Asher *et al.* 2011, supplementary information 1). Most of the intraspecific variation in the presacral vertebral counts of extant mammals reported by Asher *et al.* (2011) vary from one (majority of species) to three and the wild boar (*Sus scrofa*) has the same vertebral variation as *Galesaurus* (four elements) and individuals of the rock hyrax (*Procavia capensis*) even vary by as many as five vertebrae (Asher *et al.* 2011, supplementary information 1).

The identification of cervical vertebrae in therapsids is difficult because all presacral vertebrae in this group have free ribs. An extensive revision of therapsid axial skeletons was completed by one of us (FA) and the results showed that there are no consistent features that can aid in locating the transition between cervical and thoracic vertebrae (as in the absence/presence of articulated free ribs to the vertebrae, a consistent character in living mammals that allows differentiation from cervical to thoracic elements). Seven cervical vertebrae are identified in the subadults RC 845 and SAM-PK-K10465. The transition between the cervical and thoracic vertebrae is identified in RC 845 after a change in orientation of the transverse processes, which are directed more anteriorly; whereas the transition in SAM-PK-K10465 is after the change to a more lateral orientation of the zygapophyseal facets. Previous reports

have indicated six (Brink & Kitching 1953) and seven (Jenkins 1970, 1971) cervicals for other cynodonts.

The morphology of the axis of *Galesaurus* was first described by Parrington (1934), however the neural spine of the axis in the described specimen (UMZC T 820) was broken. Jenkins (1971) inferred an anterior convex morphology for the neural spine of the axis in *Galesaurus* by interpreting the morphology of an incomplete axial spine in *Thrinaxodon* (Jenkins 1971, fig. 2A). In the axial neural spines of both the subadult and adult specimens of *Galesaurus* in our sample, the base of the anterior margin is convex, but becomes progressively concave in the middle to upper sections. This condition of the axis spine has been reported in other cynodonts as well (e.g. Oliveira *et al.* 2010).

The anterior and posterior margins of the scapular blade are only incipiently projected in the subadults, but the blade grows into a robust element with laterally projecting anterior and posterior margins in the adults. The lateral bony ridge extending from the dorsal edge of the supracoracoid fossa to the dorsal margin of the scapula blade in the subadults (Fig. 7A, B) probably provided additional attachment for the M. infraspinatus. Interestingly, this structure was not observed in any of the adult specimens. The reason why this ridge would be present in the subadults and not the adults cannot be determined at this time. New specimens will hopefully shed more light on this feature in the future.

The shaft of the adult humerus has prominent dorsal ridges for the M. latissimus dorsi (Fig. 9B, C). A ridge for the M. teres minor separates the broad fossa on the anterolateral surface of the deltopectoral crest from the humeral head. The insertion for the M. dorsoscapularis (i.e. M. deltoideus) is slightly distal in posteromedial view whereas a shallow, but broad, fossa is present on the anterodorsal surface of the deltopectoral crest and probably indicates the origin of the M. brachialis. These ridges are poorly developed in the subadults. There is also ontogenetic variation in the development of the distal epicondyles, with a thicker entepicondyle in the subadults, but a thicker ectepicondyle in the adults.

The ilium of the adults has a slightly elongated neck and rounded iliac blade, with the blade set higher than in the subadults. These variations in the ilium were also recognized as differences between *Galesaurus* and *Thrinaxodon* by Broom (1932*b*). Jenkins (1971) inferred that the highest section of the iliac blade in cynodonts was directly above the most anterior part of the acetabulum. He was cautious with this interpretation because marginal damage was present in all the specimens in his sample. The condition inferred by Jenkins (1971) characterizes the ilium of subadult *Galesaurus*, whereas in the adults, the highest section of the blade is on the anterior lamina, in front of the acetabulum. A notable trait in this bone, represented in both the subadults and adults, is an extremely long posterior projection of the iliac blade, suggesting a strong development of the gluteal muscles with a wide area of origin for these muscles posterior to the acetabulum. The posterior projection of the ilium in cynodonts is absent in extant mammals and is interpreted here as an additional area of origin for the gluteal muscles. In contrast, these muscles attach on the iliac blade, lateral part of the sacrum and first caudal vertebrae in the dog (Evans 1993). The iliac blade in the subadults exhibits small and evenly spaced striations on the medial and dorsal surfaces, whereas the posterior surface is almost devoid of these except for a few striations just above the posteroventral edge. In the adults, the striations are more prominent on the anterior and dorsal margins whereas the medial surface of the iliac blade is uneven and may represent evidence for the presence of connective tissue in the sacroiliac joint (Jenkins 1971). The neck of the pubis is longer and the anterodorsal edge of the pubic plate is larger and more rod-like in the adults.

The femoral head of the subadults has a flat, strap-shaped edge from the head to the greater trochanter, whereas the proximal edge of the greater trochanter is slightly swollen and expands towards the femoral head. These features differ from those seen in the adults where the slope of the medial surface of the femoral head is steeper than the subadults and the proximal articulation surface is notably thicker. Additionally, the greater trochanter in the subadult femur is slightly thicker than the connecting ridge, whereas it expands dorsally and is as thick as the connecting ridge in the adults. As in the eucynodonts *Diademodon* and *Cynognathus*, the anterior and ventral surfaces distal to the lesser trochanter meet in a short thin groove (Jenkins 1971). This groove is prominent in both subadult and adult *Galesaurus*.

The condition observed in the manus of *Galesaurus* is particularly remarkable. This is the first report of variation in the manus of specimens of the same species. The phalangeal formula reported for this taxon in previous studies was 2-3-4-?4-3, revealing a definite presence of a phalangeal disc in digit III and the inferred presence of this disc in digit IV (Brink & Kitching 1951; Hopson 1995). New evidence shows heterogeneity in the phalangeal formula. Disc-like phalanges are absent in subadult SAM-PK-K10465 and is thus likely to have had a mammalian phalangeal formula: 2-3-3-3-3. In contrast, in NMQR 3716, a phalangeal disc is absent in digit III, but is present in digit IV. Moreover, SAM-PK-K10468 also presents a disc-like phalange in digit III, but the number of phalanges in the digit is three (instead of the expected four), being the only case recorded for any therapsid.

The metacarpals and phalanges of the manus are clearly more developed than the corresponding elements of the pes, as shown in subadult BP/1/4506. Thus, the

metacarpals differ from the corresponding metatarsals and range from 2% (in digit II, a unique case with the metatarsal longer than the metacarpal) to 30% for digit I. Metacarpal and metatarsal III are equal in length and the remaining metacarpals are 5% longer. The difference in width between these elements is more marked ranging from 7% for digit V to 33% for digit III. Major variations in width between the metapodials are represented in digits I, II and III. Only the first phalanx of digit II is preserved in the manus of BP/1/4506. When compared with the corresponding phalanx of the pes it is 5% longer and 36% wider.

### *Comparison between* Galesaurus *and* Thrinaxodon

There are four non-mammaliaform cynodonts known from the earliest Triassic of South Africa (Abdala & Ribeiro 2010). *Thrinaxodon liorhinus* is by far the best represented, followed by *Galesaurus planiceps*, whereas *Platycraniellus elegans* is known only from two specimens and *Progalesaurus lootsbergensis* from one (Abdala & Ribeiro 2010). *Thrinaxodon* is one of the best studied cynodonts and its postcrania have been described in detail (Jenkins 1971). The postcranial morphology of *Galesaurus* has been partially described in a few previous studies (Parrington 1934; Jenkins 1971) but with the present contribution, and the wealth of recently discovered skeletons, the knowledge of this species will equal that of *Thrinaxodon*. The postcranium of *Platycraniellus* is virtually unknown, with only a single humerus associated with the skull of the holotype (Abdala 2007). Similarly, only the right scapula and left atlantal neural spine is known for *Progalesaurus* (Sidor & Smith 2004). Thus, a comprehensive postcranial comparison of Early Triassic Karoo cynodonts can only be done with *Galesaurus* and *Thrinaxodon* at this time.

Differences between *Galesaurus* and *Thrinaxodon* can be found in the vertebrae, ribs, humerus, manus and ilium. *Thrinaxodon* has a vertebral count of 27 presacrals (MMK 5265 and BP/1/7199), whereas subadult *Galesaurus* have 29 (unavailable for adults). Both taxa have six to seven dorsal ribs with a distal unexpanded portion after the costal plate. A notable difference in the proportions of the sacral region of subadult specimens of *Galesaurus* (RC 845) and *Thrinaxodon* (MMK 5265) was observed. The last presacral vertebrae are similar in size (both in length and width), but the elements of the pelvis (ilium and ischium) are clearly more developed in *Galesaurus*. The differences in the ilium are remarkable because not only is there a size variation with that of *Galesaurus* being more robust, but there is also a difference in morphology, where the ilium of *Galesaurus* is clearly more elongated than that of *Thrinaxodon*. This longitudinal extension of the ilium resulted in the incorporation of an extra vertebra to the sacrum of *Galesaurus*, bringing the total to six sacral vertebrae.

Jenkins (1971, p. 62) indicated that the vertebrae of *Galesaurus* were indistinguishable from those of *Thrinaxodon*. The postzygapophyses of the axis in *Galesaurus* are clearly more developed than those of *Thrinaxodon* and are more obliquely-oriented compared to the horizontal orientation in *Thrinaxodon*. The neural spines of the cervical vertebrae in the subadult SAM-PK-K10465 are more robust anteroposteriorly and the spine of the sixth vertebra is shorter than that in *Thrinaxodon*. However, the cervical spines in subadult RC 845 reveal a similar anteroposterior gradient to that seen in *Thrinaxodon*, with the eighth neural spine being the tallest (the eighth and ninth are taller in *Thrinaxodon*). Additionally, *Galesaurus* RC 845 has a concavity on the posterior margin of the fourth and fifth neural spines, similar to *Thrinaxodon* where the concavity is clearly present on the fifth neural spine in MMK 5265 and probably also on the fourth, although the spine is relatively incomplete. Another similarity between these specimens is in the thoracic portion of the skeleton where the neural spines posterior to the tenth vertebra are shorter, but anteroposteriorly longer than those anterior to the tenth vertebra.

Jenkins (1971, p. 66) was unable to find differences in the thoracic ribs, but Panko (2001, pp. 5–6) found a difference in the shape and characterized *Galesaurus* plates as lobate, similar to that of the basal Cynognathia, such as *Cynognathus* and *Luangwa*, and clearly different to the plates of *Thrinaxodon*, which are ovoid.

We agree with Panko (2001) and differentiate the short and rectangular plates of *Galesaurus* (e.g. SAM-PK-K10465) from the ovoid plates of *Thrinaxodon* (e.g. MMK 5265) (Fig. 18). Associated with this difference in plate morphology, is a well-defined dorsal margin in *Galesaurus* that extends for a short distance from the costal tubercle and then abruptly descends to meet the distal diaphysis. In contrast, the dorsal margins of the plates in *Thrinaxodon* descend gradually from the costal tubercle to the distal diaphysis. Costal tubercles on the thoracic and lumbar plates are remarkably reduced in *Galesaurus* compared to those of *Thrinaxodon*, which form a continual/unbroken parasagittal longitudinal ridge (Fig. 18). Panko (2001, p. 6) described the lumbar plates of *Galesaurus* as cranio-caudally long and very different from the shorter, rounded lumbar plates of *Thrinaxodon*. Our study confirms Panko's (2001) observations.

The humerus of *Galesaurus* also differs from that of *Thrinaxodon* where the distal portion of the bone in the adults has a medially expanded entepicondyle that resembles that of *Platycraniellus* (Abdala 2007). In *Thrinaxodon* (Jenkins 1971), the entepicondyle is notably thicker than

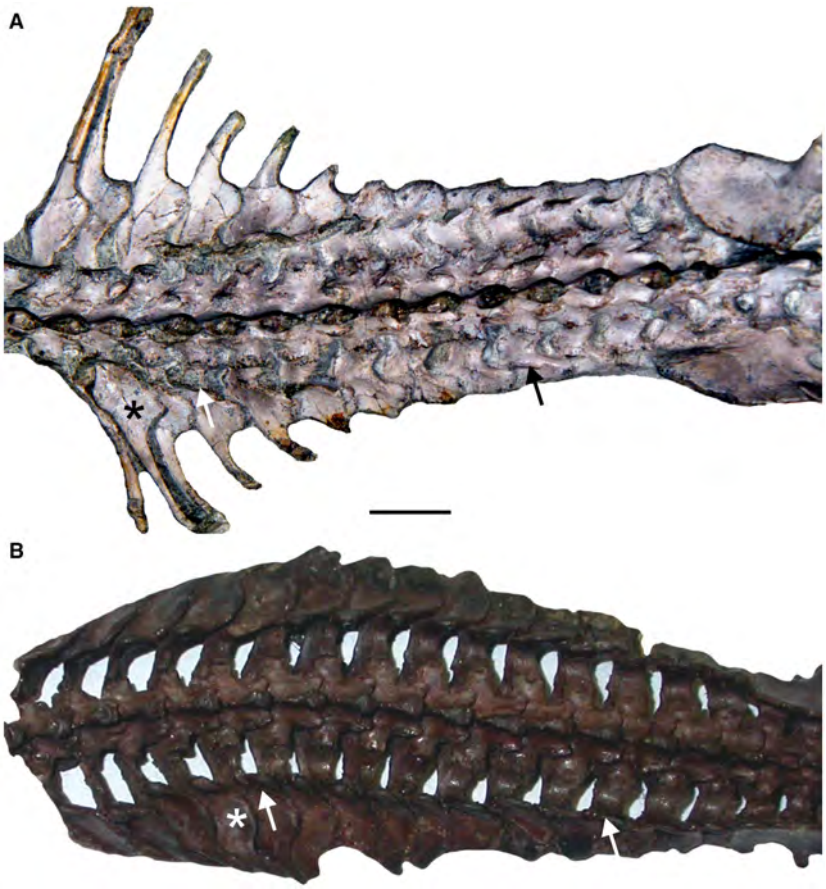


**FIG. 18.** Thoraco-lumbar skeletons. A, *Galesaurus* SAM-PK-K10465. B, *Thrinaxodon* MMK 5265. Arrows indicate costal tubercles forming a continuous parasagittal longitudinal ridge. This structure is more developed in *Thrinaxodon*. Note the rectangular thoracic plates (= lobated *sensu* Panko 2001) in *Galesaurus*, which are ovoid in *Thrinaxodon* (asterisks). Scale bar represents 20 mm. Colour online.

the ectepicondyle, a condition that is reversed in large adults of *Galesaurus* (NMQR 3542).

The manus of *Galesaurus* has four distalia, which differs from the condition seen in *Thrinaxodon*, which has a fifth distal bone (Parrington 1933; Jenkins 1971; FA pers. obs.). The digital formula of the *Thrinaxodon* manus is constrained by the presence of a disc-like phalanx in digits III and IV (observed in at least three specimens of *Thrinaxodon*; BP/1/1737; BP/1/7199; UMZC T811). In contrast, this constraint appears to have been relaxed in *Galesaurus* because the presence of these phalanges is variable (see above).

A comparison of similar-sized specimens of *Galesaurus* (RC 845) and *Thrinaxodon* (MMK 5265; see Jenkins 1971, fig. 12C) show clear differences in the ilium, with *Galesaurus* having a relatively longer iliac blade anteriorly (the posterior portion of the blade is not complete in MMK 5265). The anterior portion of the iliac blade in *Galesaurus* extends along two vertebrae, compared with one in *Thrinaxodon*. Additionally, the dorsal margin of the ilium is horizontal in nearly all of its extension in *Thrinaxodon*, whereas in *Galesaurus* it is horizontal anteriorly, but slopes down along the margin of the elongated posterior lamina.

*Limb proportions of* Galesaurus *and* Thrinaxodon

The availability of the stylopodium (humerus, femur) and zeugopodium (radius/ulna, tibia/fibula) of both *Galesaurus* and *Thrinaxodon* specimens, allowed us to analyse the ratios between these elements. The humeral and radial lengths of the same individual were measured on six specimens of *Galesaurus* (Table 3). Individuals included both subadults and adults, ranging in BSL from 67–114 mm. The ratio between the humeral and radial lengths in our sample of *Galesaurus* decreases with size (from 0.79 to 0.72; 0.81 in BP/1/4637 is uncertain; Table 3) that is, the difference in the radial and humeral lengths increases with age. In *Thrinaxodon*, however, the ratio varies from 0.68 to 0.75 in small specimens to a maximum of 0.88 in the largest specimen, showing that the ratio increases with size (Table 3) (although two adult specimens have lower ratios at 0.73 and 0.74, which could be attributed to preservational bias). This indicates that the radial and humeral lengths became more similar with age in *Thrinaxodon*. There is an ontogenetic trend of increasing differences between the humeral and radial lengths in *Galesaurus* contrasting with a (less clear) trend of equalization in the lengths of these bones in *Thrinaxodon*. The

**TABLE 3.** Length of stylopodium (humerus/femur) and zeugopodium (radius/tibia) (in mm) and ratios between these bones.

| Accession No. | BSL | HL | RL | RL/HL | FL | TL | TL/FL | HL/FL | F/H |
|---|---|---|---|---|---|---|---|---|---|
| *Galesaurus planiceps* | | | | | | | | | |
| SAM-PK-K10465 | 67 | 39 | 31 | 0.79 | 46 | 41 | 0.89 | 0.85 | 0.8 |
| RC 845 | 69 | 39 | – | – | 44 | – | – | 0.89 | – |
| 3716 | 72 | 41 | – | – | 45 | – | – | 0.91 | – |
| BP/1/4637 | 75 | ~43 | ~35 | 0.81 | 49 | 42 | 0.86 | 0.88 | 0.86 |
| BP/1/4506 | 85 | 52 | 0.37 | 0.71 | ~58 | 47 | 0.81 | 0.9 | 0.85 |
| BP/1/2513a | 90 | 55 | 40 | 0.73 | – | – | – | – | – |
| TM 83 | 94 | 49 | – | – | 58 | 51 | 0.88 | 0.84 | 0.89 |
| NMQR 3542 | 102 | ~60 | ~43 | 0.72 | 62 | 54 | 0.87 | 0.97 | – |
| NMQR 860 | 114 | 51 | 37 | 0.72 | – | – | – | – | – |
| *Thrinaxodon liorhinus* | | | | | | | | | |
| SAM-PK-K8004 | ~30 | 18 | 13 | 0.72 | 19 | – | – | 0.95 | – |
| BP/1/5372 | 37 | 20 | ~14 | 0.7 | – | – | – | – | – |
| SAM-PK-K10017 st | 42 | 20 | 15 | 0.75 | 20 | 18 | 0.9 | 1 | 0.92 |
| SAM-PK-K10017 cu | 42 | 22 | 15 | 0.68 | – | – | – | – | – |
| TM 80A | 56 | – | – | – | 28 | 26 | 0.93 | – | – |
| SAM-PK-K10607 | 66 | 29 | 25 | 0.86 | – | – | – | – | – |
| BP/1/3848 | 70 | 33 | 27 | 0.82 | – | – | – | – | – |
| BP/1/472 | 71 | 33 | 28 | 0.85 | – | – | – | – | – |
| BP/1/5208 | 73 | 32 | 28 | 0.87 | 42 | – | – | 0.76 | – |
| BP/1/7199 | 75 | 33 | 29 | 0.88 | 39 | 34 | 0.87 | 0.85 | 0.85 |
| BP/1/4331B | 75 | 37 | 27 | 0.73 | – | – | – | – | – |
| BP/1/1730 | 79 | 38 | ~28 | 0.74 | 43 | 37 | 0.86 | 0.88 | 0.82 |
| BP/1/1693 | 81 | – | 34 | – | 42 | 37 | 0.88 | – | – |
| NMQR 809 | 91 | 43 | 38 | 0.88 | 51 | – | – | 0.84 | – |
| USNM 22812 | 94 | 41 | – | – | 45 | – | – | 0.91 | – |

In both taxa, skulls 40–79% of the maximum known BSL represent subadults and 80–100%, adults.*Abbreviations*: BSL, basal skull length; cu, specimen with vertebral column curved; F/H, forelimb length/hind limb length; FL, femoral length; HL, humeral length; RL, radial length; st, specimen with vertebral column straight; TL, tibial length.

reason for the increasing difference in the lengths of these elements in *Galesaurus* appears to be that the humerus grew faster than the radius to reach a proportionately larger size, whereas the growth rates appear to have become more similar as *Thrinaxodon* aged.

The ratios between the lengths of the tibia and femur in five specimens of *Galesaurus* (Table 3) show little variation in the proportion of these bones, with the smallest specimen having a value of 0.89 and the two largest specimens having ratios of 0.87 and 0.88. The ratios in *Thrinaxodon* show a slight decrease in the length of the femur and tibia with age, with the smallest specimens having an average value of 0.92 and the two largest 0.87 (Table 3).

The ratios of humeral to femoral length in subadult *Galesaurus* (0.85 to 0.91) indicate that the femur is always the longer element (ranging from 5 to 16% longer than the humerus). The ratios of the two adults differ quite considerably from one another; 0.84 and 0.95 being the lowest and highest values in the sample (Table 3). In *Thrinaxodon* the ratio varies from 0.95–1.00 in small specimens and 0.76–0.91 in the adults, indicating that the difference in the length between femur and humerus increases towards adulthood.

It is important to highlight that the limb bones of *Galesaurus* are notably longer than those of *Thrinaxodon*. For example, the forelimbs of subadult *Galesaurus* RC 845 (BSL 64 mm) and SAM-PK-K10465 (BSL 67 mm) are only slightly shorter than the forelimbs of the largest *Thrinaxodon* NMQR 809 (BSL 91 mm) and USNM 22812 (BSL 94 mm).

### *Osteohistology*

The osteohistology of all the *Galesaurus* limb bones examined reveals early rapid growth and a decrease in growth rate later in life. Although the absence of an EFS, in the form of multiple growth marks, in the oldest individual indicates that growth had not ceased completely, the peripheral deceleration in growth indicates that it was an adult. Some studies have also suggested that the transition to slow growing tissues marks the onset of reproductive

maturity (Sander 2000; Lee & Werning 2008). The peripheral slow growing tissue type differs between *Galesaurus* and *Thrinaxodon* with lamellar-zonal bone deposited in the former and parallel-fibred bone in the latter taxon. Although lamellar-zonal bone typically grows more slowly than parallel-fibred bone, there are some patches of parallel-fibred bone in the younger individuals of *Galesaurus*, and also in parts of the oldest individual investigated (NMQR 3542), suggesting that the adult tissues grew at similar rates. The LAG within the slow growing bone tissue of the largest, oldest individual of *Galesaurus* indicates that much of the growth of this taxon (and possibly reproductive maturity) occurred within one year (i.e. prior to the first growth mark). This growth pattern is similar to that of *Thrinaxodon*, which also grew rapidly and continuously to somatic maturity within a year (Botha & Chinsamy 2005). It should be noted that a mid-cortical annulus was found in a femur in a study on the osteohistology of *Thrinaxodon* (Botha & Chinsamy 2005). However, as this growth mark was found in a single femur and growth marks were absent from the rest of the 10 elements, Botha & Chinsamy (2005) considered the general growth pattern of *Thrinaxodon* to be uninterrupted to adulthood. It is possible that the individual exhibiting the annulus was born late in the breeding season resulting in the unfavourable growing season (represented by the annulus) occurring earlier in its growth compared to other individuals. *Galesaurus* NMQR 3542, which is a skeletally mature individual, differs from this *Thrinaxodon* individual in that all the bones exhibit a LAG within the slow growing peripheral bone tissue, after adulthood had already been reached.

In a study on the osteohistology of latest Permian and earliest Triassic therapsids, Botha-Brink *et al.* (2016) suggested that reaching somatic and reproductive maturity within one year was advantageous in a harsh, unpredictable environment such as that reconstructed for the Early Triassic, following the PTME. An early onset of reproductive maturity would have increased survival rates in an environment with shortened life expectancies (Botha-Brink *et al.* 2016). This may have aided in the survival of both *Galesaurus* and *Thrinaxodon*.

The microanatomy of the *Galesaurus* forelimb elements revealed compact, thick cortices indicating that the forelimb was strong and robust, and able to withstand the strain of powerful muscles. The prominent Sharpey's fibres in all three elements of NMQR 3542 provide further support for the presence of strong muscles in the *Galesaurus* forelimb. The hind limb revealed thinner cortices, further suggesting that it was the forelimb that was mostly involved in digging. When compared with *Thrinaxodon*, the overall compactness of the forelimb elements in *Galesaurus* is only slightly higher than those of *Thrinaxodon* (humerus BP/1/5208 Cg = 0.845; radius BP/1/4282a Cg = 0.738; ulna BP/1/4282b Cg = 0.808). However, the cortical thickness between the two genera is notably different (Fig. 18). The forelimb elements of *Galesaurus* are substantially thicker (humerus $K = 0.13$; radius $K = 0.23$; ulna $K = 0.14$) compared to those of *Thrinaxodon* (BP/1/5208 humerus $K = 0.41$; radius BP/1/4282a $K = 0.51$; ulna BP/1/4282b $K = 0.43$) showing that the forelimb of the former was stronger and able to resist high reaction forces produced by powerful interactions with the substrate.

## Galesaurus *palaeoecology*

*Galesaurus* was a relatively small (maximum BSL 114 mm) insectivorous non-mammaliaform cynodont. It was more robust and slightly larger, but otherwise similar in both morphology and osteohistology to its contemporaneous sister taxon *Thrinaxodon*. However, *Thrinaxodon* appears to be remarkably more abundant than *Galesaurus* with 114 and 35 specimens having been recovered, respectively (taken from data in South African museum collections). The biostratigraphical ranges also differ. The lowest occurrence of both taxa is within the lowermost LAZ from the uppermost Palingkloof Member of the Balfour Formation (Smith & Botha 2005; Smith & Botha-Brink 2014), but the range of *Thrinaxodon* extends through the entire LAZ, whereas *Galesaurus* disappears in the lower half of the LAZ (Neveling 2004; Botha & Smith 2006). However, only two *Thrinaxodon* specimens have been found above the Swartberg member of the Katberg Formation near the uppermost boundary of the LAZ (Neveling 2004). The rest of the specimens were found in the Palingkloof Member, Balfour Formation and overlying lower to middle Katberg Formation at similar stratigraphical levels to *Galesaurus* (Botha & Smith 2006). With more collecting efforts, it is possible that *Galesaurus* may be recovered at higher stratigraphical levels in the LAZ in future, given that only two *Thrinaxodon* specimens have been recovered from the uppermost part of this assemblage zone, despite its abundance in the lower levels.

Although previous studies have suggested that *Thrinaxodon* was an active burrower (Damiani *et al.* 2003; Fernandez *et al.* 2013; Iqbal 2015; Jasinoski & Abdala 2017*b*) the relatively slender, thin bones of the forelimb do not provide much support for counteracting the strain of large, powerful muscles that are generally required for active forelimb digging. Thus, it is possible that *Thrinaxodon* engaged in other forms of digging, perhaps using other parts of the body to excavate burrows. Alternatively, *Thrinaxodon* may have made use of burrows excavated by other taxa, and perhaps only rarely excavated its own burrows. In contrast, the thick, robust bones of *Galesaurus* reveal that it was well adapted for forelimb digging (Fig. 19). The

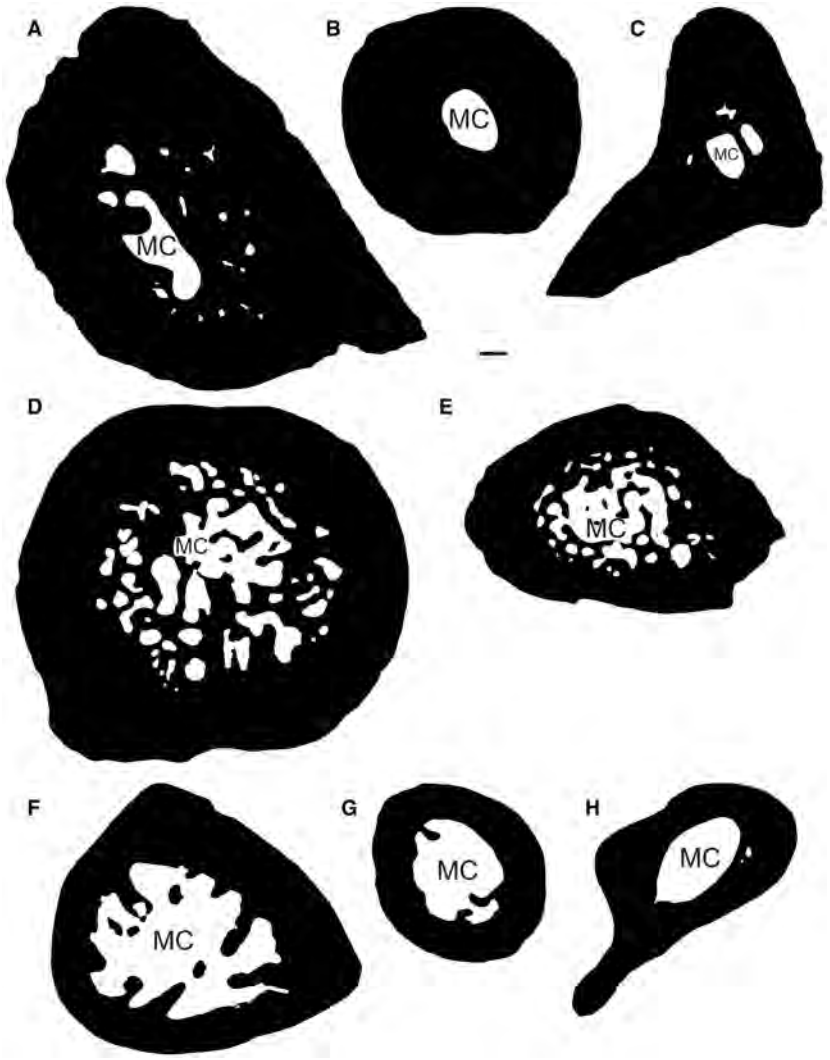


**FIG. 19.** Cross-sections through the midshaft of *Galesaurus planiceps* NMQR 3542 (A, humerus; B, radius; C, ulna; D, femur; E, tibia) and *Thrinaxodon liorhinus* (F, humerus BP/1/5208; G, radius BP/1/4282a; H, ulna BP/1/4282b) forelimbs showing the relatively thicker cortices in the *Galesaurus* forelimb compared to the hind limb and forelimb of *Thrinaxodon*. *Abbreviation*: MC, medullary cavity. Scale bar represents 500 μm.

morphology of *Galesaurus* does not reveal any prominent specializations for digging, such as a dorsoventrally expanded scapula blade, a long olecranon process on the ulna or notably long unguals (Hildebrand 1985), which are adaptations typical of a subterranean lifestyle where an animal spends most of its time underground. There are numerous extant vertebrates with a more general morphology that excavate burrows diurnally or seasonally for shelter or reproduction. *Galesaurus* does have other morphological features found in fossorial and semi-fossorial taxa such as thick, robust forelimbs, a large humeral ectepicondyle that is 35% larger than the entepicondyle (equivalent to the lateral epicondyle in extant mammals), a wide humeral distal epiphysis (humeral length to distal width 53%, see Hildebrand 1985) and a robust, elongated ilium.

Additionally, *Galesaurus* has six sacral vertebrae (a feature not observed in other cynodonts) compared to five in *Thrinaxodon*, giving *Galesaurus* a stronger, more stable pelvis, which is important for providing a steady, rigid base to support the animal's weight during forelimb digging. The longer ilium in *Galesaurus* would have also provided more surface area for the gluteal muscles, thus creating a stronger brace to counteract the forces exhibited during forelimb digging (Hildebrand 1985). Although several *Thrinaxodon* specimens have been recovered from burrows (e.g. Damiani *et al.* 2003; Fernandez *et al.* 2013; Iqbal 2015; Jasinoski & Abdala 2017*b*) there are more features in *Galesaurus* (e.g. an extra sacral vertebra, thick bone walls, robust limb bones, stout unguals, and an elongated ilium) than *Thrinaxodon* to indicate that the former taxon was fully capable of actively digging burrows.

In a recent study on possible parental care in *Galesaurus* and *Thrinaxodon*, Jasinoski & Abdala (2017*b*) proposed that social behaviour was more prevalent in *Thrinaxodon* and that this trait may have aided in the survival of the species. They studied 35 *Galesaurus* and 104 *Thrinaxodon* specimens and found two and seven

aggregations, respectively. Given that only one of the seven *Thrinaxodon* aggregations contains juveniles, they proposed that *Thrinaxodon* subadults and adults formed social aggregations more often than did *Galesaurus* (Jasinoski & Abdala 2017*b*). The discovery of *Galesaurus* NMQR 135 representing an aggregation brings the total of known aggregations to three amongst 35 specimens. When the percentage of aggregations amongst the total number of specimens is assessed, the proportion is similar with 7% of the specimens representing aggregations in *Thrinaxodon* and 9% in *Galesaurus*.

*Galesaurus* was larger, more robust and better equipped at excavating burrows compared to *Thrinaxodon*. The two taxa also appear to have had similar growth patterns. Apart from a slight sexual dimorphism in *Galesaurus*, its morphology and growth patterns are essentially the same as *Thrinaxodon*. Thus, there is no clear reason to explain why *Thrinaxodon* was more abundant than *Galesaurus*. *Galesaurus* actually appears to have been better adapted to its environment by being a sturdy animal capable of excavating its own burrows and thus providing its own shelter. However, Jasinoski & Abdala (2017*a*, *b*) suggested that parental care lasted longer in *Galesaurus* and perhaps it was *Thrinaxodon*'s ability to reach independence at younger ontogenetic stages that resulted in it being relatively more successful.

*Acknowledgements.* The authors are grateful to the following researchers and collection managers for access to the specimens studied: R. Smith and S. Kaal (Iziko); B. Rubidge, M. Raath and B. Zipfel (Evolutionary Studies Institute, University of the Witwatersrand); B. S. Rubidge (Rubidge Collection); H. Fourie and S. Potze (Ditsong Museum); J. Clack and R. Symonds (University Museum of Zoology, Cambridge). We thank the fossil preparators of the Evolutionary Studies Institute, University of the Witwatersrand, Iziko Museums of South Africa, Cape Town and the National Museum, Bloemfontein for manually preparing the specimens. We are grateful to L. Gaetano and S. Kümmell for commenting on a first draft. Final reviews by L. Gaetano, A. Huttenlocker and an unknown reviewer are especially appreciated. This work was supported by the National Research Foundation (UID 98819, 95980 to JBB). Further support was provided by the Palaeontological Scientific Trust (PAST) and its Scatterlings of Africa programmes and DST/NRF Centre of Excellence in Palaeosciences to JBB and NRF and Conicet, Argentina to FA.

*Editor*. Kenneth Angielczyk

## REFERENCES

ABDALA, F. 1999. Elementos postcraneanos de *Cynognathus* del Triásico Inferior de la Provincia de Mendoza, Argentina. Consideraciones sobre la morfología del húmero en cinodontes. *Revista Española de Paleontología*, **14**, 13–24.

—— 2003. Galesaurid cynodonts from the Early Triassic of South Africa: another example of conflicting distribution of characters in non-mammalian cynodonts. *South African Journal of Science*, **99**, 95–96.

—— 2007. Redescription of *Platycraniellus elegans* (Therapsida, Cynodontia) from the Lower Triassic of South Africa, and the cladistic relationships of Eutheriodonts. *Palaeontology*, **50**, 591–618.

—— and DAMIANI, R. 2004. Early development of the mammalian superficial masseter muscle in cynodonts. *Palaeontologia Africana*, **40**, 23–29.

—— and GIANNINI, N. P. 2002. Chiniquodontid cynodonts: systematic and morphometric considerations. *Palaeontology*, **45**, 1151–1170.

—— and RIBEIRO, A. M. 2010. Distribution and diversity patterns of Triassic cynodonts (Therapsida, Cynodontia) in Gondwana. *Palaeogeography, Palaeoclimatology, Palaeoecology*, **286**, 202–217.

—— CISNEROS, J. C. and SMITH, R. M. H. 2006. Faunal aggregation in the Early Triassic Karoo Basin: earliest evidence of shelter-sharing among tetrapods? *Palaios*, **21**, 507–512.

AMPRINO, R. 1947. La structure du tissu osseux envisagee comme expression de differences dans la vitesse de l'accroissement. *Archives de Biologie*, **58**, 315–330.

ASHER, R. J., LIN, K. H., KARDJILOV, N. and HAUTIER, L. 2011. Variability and constraint in the mammalian vertebral column. *Journal of Evolutionary Biology*, **24**, 1080–1090.

BLOB, R. W. 2001. Evolution of hind limb posture in non-mammalian therapsids: biomechanical tests of paleontological hypotheses. *Paleobiology*, **27**, 14–38.

—— 2006. Scaling of the hind limb skeleton in cynognathian cynodonts: implications for ontogeny and the evolution of mammalian endothermy. 410–431. *In* CARRANO, M. T., GAUDIN, T. J., BLOB, R. W. and WIBLE, J. R. (eds). *Amniote paleobiology: perspectives on the evolution of mammals, birds, and reptiles*. University of Chicago Press, 448 pp.

BONAPARTE, J. F. 1963. Descripción del esqueleto postcraneano de *Exaeretodon*. *Acta Geológica Lilloana*, **4**, 5–52.

BOTHA, J. and CHINSAMY, A. 2005. Growth patterns of *Thrinaxodon liorhinus*, a non-mammalian cynodont from the Lower Triassic of South Africa. *Palaeontology*, **48**, 385–394.

—— and SMITH, R. M. H. 2006. Rapid vertebrate recuperation in the Karoo Basin of South Africa following the End-Permian extinction. *Journal of African Earth Sciences*, **45**, 502–514.

—— ABDALA, F. and SMITH, R. M. H. 2007. The oldest cynodont: new clues on the origin and early diversification of the Cynodontia. *Zoological Journal of the Linnean Society*, **149**, 477–492.

BOTHA-BRINK, J., ABDALA, F. and CHINSAMY, A. 2012. Bone histology and radiation of Permo-Jurassic non-mammaliaform cynodonts. 223–246. *In* CHINSAMY, A. (ed.) *The forerunners of mammals: radiation, biology, histology*. Indiana University Press, 330 pp.

—— CODRON, D., HUTTENLOCKER, A. K., ANGIELCZYK, K. D. and RUTA, M. 2016. Breeding young as a survival strategy during earth's greatest mass extinction. *Scientific Reports*, **6**, 24053.

BRINK, A. S. and KITCHING, J. W. 1951. Studies of Karroo Reptiles. II. On *Leavachia*, a procynosuchid cynodont from the Middle *Cistecephalus* Zone. *South African Journal of Science*, **48**, 342–347.

—— —— 1953. On some new *Cynognathus* Zone specimens. *Palaeontologia Africana*, **1**, 29–48.

BROOM, R. 1932*a*. The cynodont genus *Galesaurus*. *Annals of the Natal Museum*, **7**, 61–66.

—— 1932*b*. *The mammal-like reptiles of South Africa and the origin of mammals*. H. F. & G. Witherby, London, 376 pp.

BUTLER, E. 2009. The postcranial skeleton of the Early Triassic non-mammalian Cynodont *Galesaurus planiceps*: implications for biology and lifestyle. Unpublished MSc thesis, University of the Free State, Bloemfontein, 152 pp.

CORMACK, D. H. 1987. *Ham's histology*. J. B. Lippincott Co., London, 866 pp.

CURREY, J. D. and ALEXANDER, R. MCN. 1985. The thickness of the walls of tubular bone. *Journal of Zoology*, **206**, 453–468.

DAMIANI, R., MODESTO, S., YATES, A. and NEVELING, J. 2003. Earliest evidence of cynodont burrowing. *Proceedings of the Royal Society of London B*, **270**, 1747–1751.

EVANS, H. E. 1993. *Miller's anatomy of the dog*. 3rd edn. W. B. Saunders Company, Philadelphia, 1113 pp.

FERNANDEZ, V., ABDALA, F., CARLSON, K. J., COLLINS COOK, D., RUBIDGE, B. S., YATES, A. and TAFFOREAU, P. 2013. Synchrotron reveals Early Triassic odd couple: injured amphibian and aestivating therapsid share burrow. *Plos One*, **8**(6), e64978.

FRANCILLON-VIEILLOT, H., BUFFRÉNIL, V. DE, CASTANET, J., GERAUDIE, J., MEUNIER, F. J., SIRE, J. Y., ZYLBERBERG, L. and RICQLÈS, A. DE 1990. Microstructure and mineralization of vertebrate skeletal tissues. 471–548. *In* CARTER, J. G. (ed.) *Skeletal biomineralization: patterns, processes and evolutionary trends*. Van Nostrand Reinhold, New York, 471–530.

GAETANO, L. C., ABDALA, F. and GOVENDER, R. 2017. The postcranial skeleton of the Lower Jurassic *Tritylodon longaevus* from Southern Africa. *Ameghiniana*, **54**, 1–35.

GIRONDOT, M. and LAURIN, M. 2003. Bone profiler: a tool to quantify, model, and statistically compare bone-section compactness profiles. *Journal of Vertebrate Paleontology*, **23**, 458–461.

GOW, C. 2001. A partial skeleton of the tritheledontid *Pachygenelus* (Therapsida: Cynodontia). *Palaeontologia Africana*, **37**, 93–97.

HAUGHTON, S. H. 1924. On Cynodontia from the Middle Beaufort beds of Harrismith, Orange Free State. *Annals of the Transvaal Museum*, **11**, 74–92.

HILDEBRAND, M. 1985. Digging of quadrupeds. 89–109. *In* HILDEBRAND, H., BRAMBLE, D. M., LIEM, K. L. and WAKE, D. B. (eds). *Functional vertebrate morphology*. Belknap Press, 430 pp.

HOPSON, J. A. 1995. Patterns of evolution in the manus and pes of non-mammalian therapsids. *Journal of Vertebrate Paleontology*, **15**, 615–639.

—— and KITCHING, J. W. 1972. A revised classification of cynodonts (Reptilia: Therapsida). *Palaeontologia Africana*, **14**, 71–85.

—— —— 2001. A probainognathian cynodont from South Africa and the phylogeny of nonmammalian cynodonts. *Bulletin Museum of Comparative Zoology*, **154**, 5–35.

HUTTENLOCKER, A. K. and BOTHA-BRINK, J. 2014. Bone microstructure and the evolution of growth patterns in Permo-Triassic therocephalians (Amniota, Therapsida) of South Africa. *PeerJ*, **2**, e325.

IQBAL, S. 2015. The functional morphology and internal structure of the forelimb of the Early Triassic non-mammaliaform cynodont *Thrinaxodon liorhinus*. Unpublished MSc thesis, University of the Witwatersrand, Johannesburg, 72 pp.

JASINOSKI, S. C. and ABDALA, A. F. 2017*a*. Cranial ontogeny of the Early Triassic basal cynodont *Galesaurus planiceps*. *Anatomical Record*, **300**, 353–381.

—— —— 2017*b*. Aggregations and parental care in the Early Triassic basal cynodonts *Galesaurus planiceps* and *Thrinaxodon liorhinus*. *PeerJ*, **5**, e2875.

—— —— and FERNANDEZ V. 2015. Ontogeny of the Early Triassic cynodont *Thrinaxodon liorhinus* (Therapsida): cranial morphology. *The Anatomical Record*, **298**, 1440–1464.

JENKINS, F. 1970. The Chañares (Argentina) Triassic reptile fauna. VII. The postcranial skeleton of the traversodontid *Massetognathus pascuali* (Therapsida-Cynodontia). *Breviora*, **352**, 1–28.

—— 1971. The postcranial skeleton of African cynodonts. *Bulletin of the Peabody Museum of Natural History*, **36**, 1–216.

KAMMERER, C. F., FLYNN, J. J., RANIVOHARIMANANA, L. and WYSS, A. R. 2008. New material of *Menadon besairiei* (Cynodontia: Traversodontidae) from the Triassic of Madagascar. *Journal of Vertebrate Paleontology*, **28**, 445–462.

KEMP, T. S. 1969. The atlas-axis complex of the mammal-like reptiles. *Journal of the Zoological Society of London*, **159**, 223–248.

—— 1980*a*. The primitive cynodont *Procynosuchus*: structure, function and evolution of the postcranial skeleton. *Philosophical Transactions of the Royal Society of London*, **288**, 217–258.

—— 1980*b*. Aspects of the structure and functional anatomy of the Middle Triassic cynodont *Luangwa*. *Journal of Zoology*, **191**, 193–239.

LAI, P. H., BIEWENER, A. A. and PIERCE, S. E. 2018. Three-dimensional mobility and muscle attachments in the pectoral limb of the Triassic cynodont *Massetognathus pascuali* (Romer, 1967). *Journal of Anatomy*, **232**, 383–406.

LAURIN, M., CANOVILLE, A. and GERMAIN, D. 2011. Bone microanatomy and lifestyle: a descriptive approach. *Comptes Rendus Palevol*, **10**, 381–402.

LEE, A. H. and WERNING, S. 2008. Sexual maturity in growing dinosaurs does not fit reptilian growth models. *Proceedings of the National Academy of Sciences*, **105**, 582–587.

LIU, J. and OLSEN, P. 2010. The phylogenetic relationships of Eucynodontia (Amniota: Synapsida). *Journal of Mammalian Evolution*, **17**, 151–176.

—— SCHNEIDER, V. P. and OLSEN, P. E. 2017. The postcranial skeleton of *Boreogomphodon* (Cynodontia: Traversodontidae) from the Upper Triassic of North Carolina, USA and the comparison with other traversodontids. *PeerJ*, **5**, e3521.

MARGERIE, E. DE, CUBO, J. and CASTANET, J. 2002. Bone typology and growth rate: testing and quantifying 'Amprino's rule' in the mallard (*Anas platyrhynchos*). *Comptes Rendus Biologies*, **325**, 221–230.

MÜLLER, J., SCHEYER, T. M., HEAD, J. J., BARRETT, P. M., WERNERBURG, I., ERICSON, P. G. P., POL, D. and SÁNCHEZ-VILLAGRA, M. R. 2010. Homeotic effects, somitogenesis and the evolution of vertebral numbers in recent and fossil amniotes. *Proceedings of the National Academy of Sciences*, **107**, 2118–2123.

NARITA, Y. and KURATANI, S. 2005. Evolution of the vertebral formulae in mammals: a perspective on developmental constraints. *Journal of Experimental Zoology (Molecular Development Evolution)*, **304B**, 91–106.

NEVELING, J. 2004. *Stratigraphic and sedimentological investigation of the contact between the Lystrosaurus and the Cynognathus Assemblage Zones (Beaufort Group: Karoo Supergroup). Bulletin 137*. Council for Geoscience, Pretoria, 165 pp.

OLIVEIRA, T. V. 2010. Postura e locomoção em cinodontes do Triássico Sul-Americano: um estudo de caso baseado em *Trucidocynodon riograndensis* Oliveira, Soares & Schultz, 2010 (Triássico Superior, Formação Santa Maria, Bacia do Paraná; Rio Grande do Sul, Brasil). Unpublished PhD thesis, Universidade do Rio Grande do Sul, Porto Alegre, 212 pp.

—— and SCHULTZ, C. L. 2016. Functional morphology and biomechanics of the cynodont *Trucidocynodonrio grandensis* from the Triassic of Southern Brazil: pectoral girdle and forelimb. *Acta Paleontologica Polonica*, **61**, 377–386.

—— —— and SOARES M. B. 2007. O esqueleto pós-craniano de *Exaeretodon riograndensis* Abdala *et al.* (Cynodontia, Traversodontidae). *Revista Brasileira de Paleontologia*, **10**, 79–94.

—— —— —— 2009. A partial skeleton of *Chiniquodon* (Cynodontia Chiniquodontidae) from the Brazilian Middle Triassic. *Revista Brasileira de Paleontologia*, **12**, 113–122.

—— SOARES, M. B. and SCHULTZ, C. L. 2010. *Trucidocynodonrio grandensis* gen. nov.et sp. nov. (Eucynodontia), a new cynodont from the Brazilian Upper Triassic (Santa Maria Formation). *Zootaxa*, **2382**, 1–71.

OWEN, R. 1859. On some reptilian remains from South Africa. *New Philosophical Journal*, **10**, 1–289.

PANKO, L. J. 2001. Evolution and functional morphology of the axial skeleton in the Synapsida. Unpublished PhD thesis, The University of Chicago, 250 pp.

PARRINGTON, F. R. 1933. On the Cynodont reptile *Thrinaxodon liorhinus* Seeley. *Annals & Magazine of Natural History*, **10**, 16–24.

—— 1934. On the cynodont genus *Galesaurus*, with a note on the functional significance of the changes in the evolution of the theriodont skull. *Annals & Magazine of Natural History*, **10**, 38–67.

RICQLÈS, A. DE, MEUNIER, J., CASTANET, J. and FRANCILLON-VIEILLOT, H. 1991. Comparative microstructure of bone. 1–77. *In* HALL, B. K. (ed.) *Bone. 3 Bone matrix and bone specific products*. CRS Press, Boca Raton.

ROWE, T. 1988. Definition, diagnosis, and origin of Mammalia. *Journal of Vertebrate Paleontology*, **8**, 241–264.

RUBIDGE, B. S. 2005. Re-uniting lost continents–fossil reptiles from the ancient Karoo and their wanderlust. *South African Journal of Geology*, **108**, 135–172.

—— and SIDOR, C. A. 2001. Evolutionary patterns among Permo-Triassic therapsids. *Annual Review of Ecology & Systematics*, **32**, 449–480.

RUTA, M., BOTHA-BRINK, J., MITCHELL, S. A. and BENTON, M. J. 2013. The radiation of cynodonts and the ground plan of mammalian morphological diversity. *Proceedings of the Royal Society B*, **280**, 20131865.

SANDER, P. M. 2000. Longbone histology of the Tendaguru sauropods: implications for growth and biology. *Paleobiology*, **26**, 466–488.

SIDOR, C. A. and SMITH, R. M. H. 2004. A new galesaurid (Therapsida: Cynodontia) from the Lower Triassic of South Africa. *Palaeontology*, **47**, 535–556.

SIGURDSEN, T., HUTTENLOCKER, A. K., MODESTO, A. P., ROWE, T. B. and DAMIANI, R. 2012. Reassessment of the morphology and paleobiology of the therocephalian *Tetracynodon darti* (Therapsida), and the phylogenetic relationships of Baurioidea. *Journal of Vertebrate Paleontology*, **32**, 1113–1134.

SMITH, R. M. H. and BOTHA, J. 2005. The recovery of terrestrial vertebrate diversity in the South African Karoo Basin after the end-Permian extinction. *Comptes Rendus Palevol*, **4**, 555–568.

—— and BOTHA-BRINK, J. 2014. Sedimentological and taphonomic evidence for drought-induced die-offs during the Permo-Triassic mass extinction in the main Karoo Basin, South Africa. *Palaeogeography, Palaeoclimatology, Palaeoecology*, **312**, 40–53.

STARCK, J. M. and CHINSAMY, A. 2002. Bone microstructure and developmental plasticity and birds and other dinosaurs. *Journal of Morphology.*, **254**, 232–246.

SUES, H.-D. and JENKINS, F. A. Jr. 2006. The postcranial skeleton of *Kayentatherium wellesi* from the Lower Jurassic Kayenta Formation of Arizona and phylogenetic significance of postcranial features in tritylodontid cynodonts. 114–152. *In* CARRANO, M. T., GAUDIN, T. J., BLOB, R. W. and WIBLE, J. R. (eds). *Amniote paleobiology: perspectives on the evolution of mammals, birds, and repiles*. University of Chicago Press, 448 pp.

WEST, G. B., BROWN, J. H. and ENQUIST, B. J. 2001. A general model for ontogenetic growth. *Nature*, **413**, 628–631.

WIBLE, J. R. 1991. Origin of Mammalia: the craniodental evidence reexamined. *Journal of Vertebrate Paleontology*, **11**, 1–28.